The positions of the "pre-edge" peak at 8985 eV for the various Cu(I) complexes are in general accord with the predictions of ligand field splitting of copper 4p orbitals as a function of site geometry

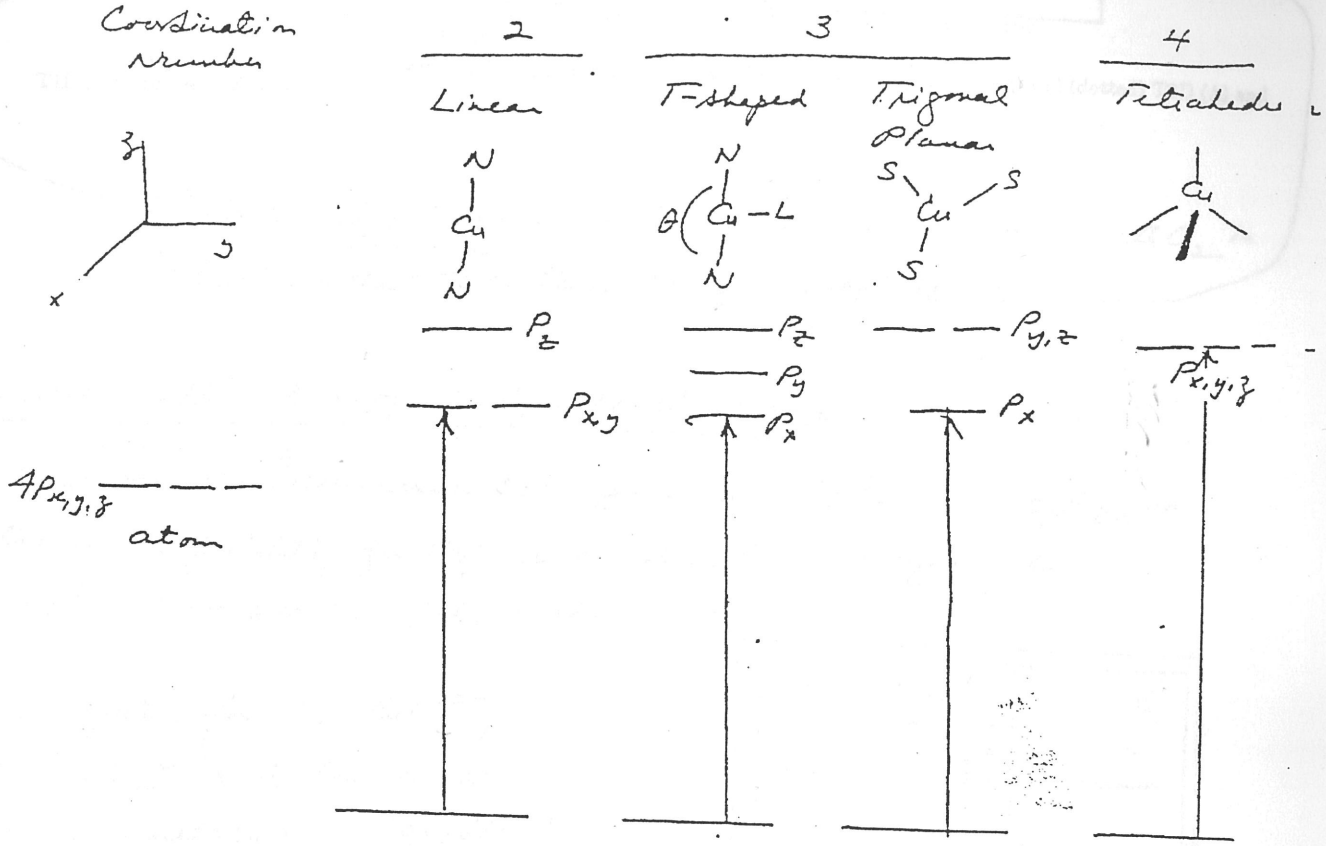

Assignment of 8985 eV "pre-edge" maximum in Cu(I) complexes

However, should include hybridization of 4s + 4p orbitals

Application of these results to laccase

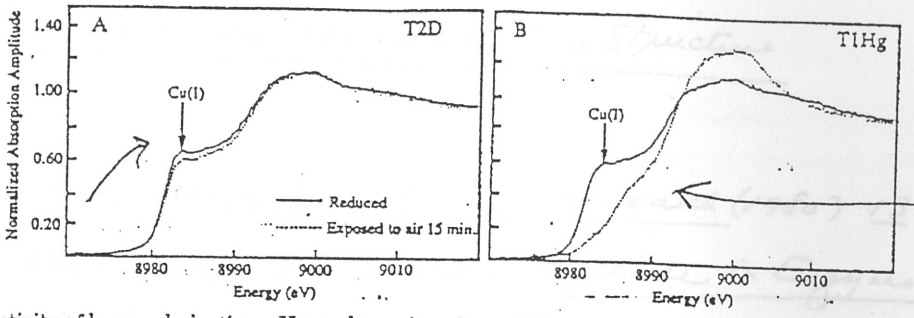

O_2 reactivity of laccase derivatives. X-ray absorption edges of fully reduced (solid) and air-exposed (dotted) T2D (A) and T1Hg (B) laccase derivatives.

a) Evidence that T3 center in Cu(I) and does not react with O_2 in T2D laccase

b) Evidence that T3 center in T1 Hg reacts with O_2

A recent application of L edge spectroscopy

L edges in copper(II) complexes correspond to $2p^6 3d^9 \rightarrow 2p^5 3d^{10}$ transitions of Cu(II); for Copper(I) complex, they correspond to $2p^6 3d^{10} \rightarrow 2p^5 3d^{10} 4s^1$ (weaker)

L edge spectra for D_{2d} $CuCl_4^{2-}$, D_{4h} $CuCl_4^{2-}$ and blue copper site in plastocyanin (oxidized and reduced).

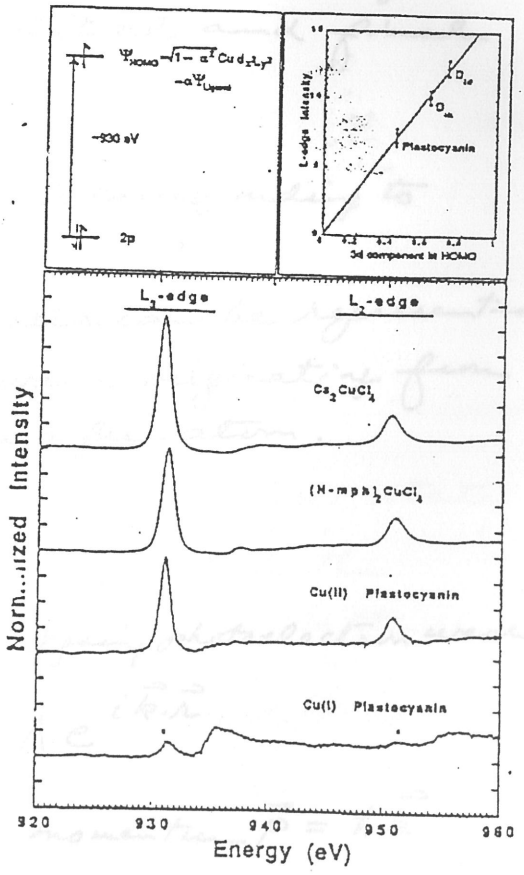

Intensity edge absorption should be proportional to $1-\alpha^2$, the $3d_{x^2-y^2}$ character in the half-occupied HOMO

$\Psi_{HOMO} = \sqrt{1-\alpha^2}\, Cu\, d_{x^2-y^2} - \alpha\, \Phi_{ligand}$

Ref S. J. George, M. D. Lowery, E. I. Solomon & S. P. Cramer, JACS (1993)

EXAFS ≡ Extended X-ray Absorption Fine Structure

References:

Kon-Keng Teo, Accounts of Chemical Research (1980) 13, 412-419;

Sunney I. Cha and Ronald C. Gamble, Methods in Enzymology, Vol. LIV, 323-345 (1978).

EXAFS refers to the sinusoidal variation of the X-ray absorption as a function of photon energy beyond an absorption edge; arises from constructive and destructive interference between outgoing photoelectron wave and incoming electron wave back scattered from neighboring atoms.

Probability that an X-ray photon will be absorbed by a core electron depends on both the initial and final states of the electron

Initial state: localized core level corresponding to the absorption edge.

Final state: ejected photoelectron can be represented by an outgoing spherical wave originating from X-ray absorbing atom, if it is a free atom.

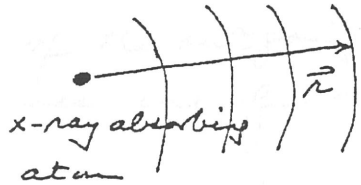

← outgoing photoelectron wave

$$\psi_i \sim A e^{i\vec{k}\cdot\vec{r}}$$

where $\vec{k}$ ≡ wave vector. Recall momentum $\vec{p} = \hbar\vec{k}$

Since $p^2 = \hbar^2 k^2 = 2m_e(E - E_0)$

where E = energy of X-ray photon

E_0 = dissociation energy for electron
(critical energy necessary to free bound electron)

$$|k| = \left[\frac{2m_e(E-E_0)}{\hbar^2}\right]^{1/2}$$

However, if absorbing atom is surrounding by a neighboring atom, the outgoing photoelectron wave will be backscattered by the neighboring atom, producing an <u>incoming</u> electron wave. Final state is then the sum of the outgoing and the incoming wave

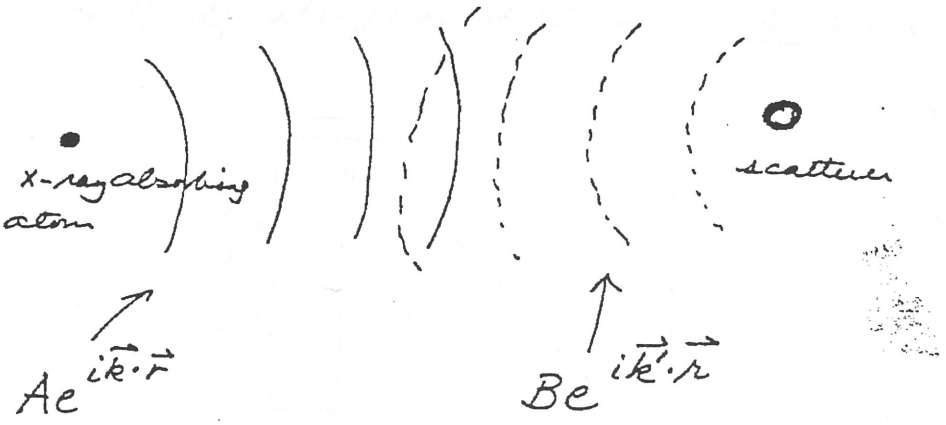

$$\psi_f \sim Ae^{i\vec{k}\cdot\vec{r}} + Be^{i\vec{k}'\cdot\vec{r}}$$

If there are more than 1 neighboring atoms, final state is the sum of the outgoing wave and all the incoming waves, one for each neighboring scatterer.

<u>Interference</u> between the outgoing wave and incoming wave(s) give rise to sinusoidal variation in the absorption coefficient <u>vs</u> E (energy of X-ray photon) $\Rightarrow$ EXAFS

This modulation of the absorption coefficient should depend on the nature of the scatterer(s), i.e., element, its charge etc., as well as its distance away from the X-ray absorbing atom (R). So EXAFS offers complementary information about a metal site, when applied to metalloproteins. Whereas the absorption edge (and XANES) is often useful in ascertaining the oxidation state, degree of covalency, the symmetry of the metal center as well as the nature of the surrounding ligands, the distance between the metal center and ligand atoms may be obtained from analysis of EXAFS.

Example Fe K-edge absorption spectrum of rubredoxin

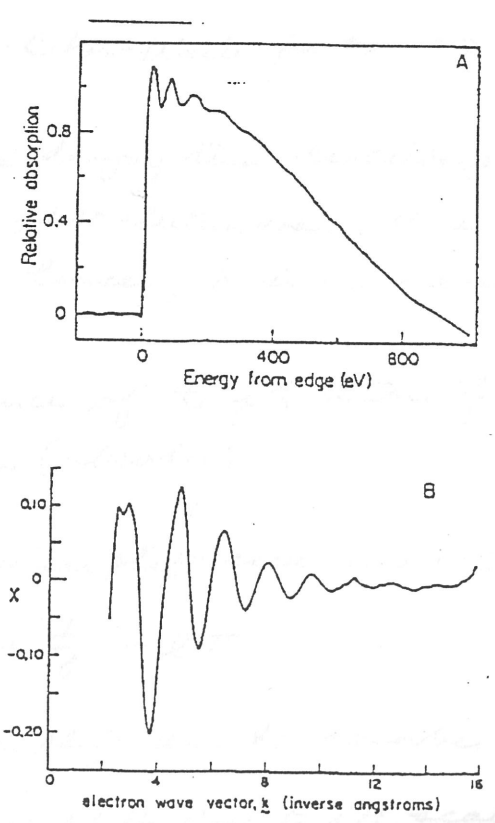

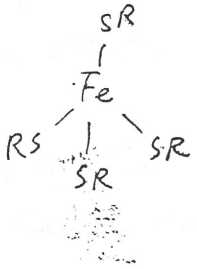

[redacted]. Fe K-edge absorption spectrum of rubredoxin. In (A), the absorption vs. X-ray energy is presented. These data have been corrected for absorption from other components (see text for details). In (B) the unnormalized EXAFS contribution, χ, is shown as a function of the wave vector, k. [Courtesy of D. Sayers and B. Bunker, University of Washington, Seattle (1976) (unpublished).]

Theory of EXAFS

$$\chi(k) = \sum_j N_j \cdot F_j(k) \cdot e^{-2\sigma_j^2 k^2} \cdot \frac{e^{-2r_j/\lambda}}{k r_j^2} \cdot \sin(2kr_j + \phi_j(k))$$

back scattering.

absorption efficiency

momentum

where $F_j(k) \equiv$ backscattering amplitude from each of the N_j neighboring atoms of type j

$N_j \equiv$ number of neighboring atoms of type j

$\sigma_j \equiv$ Debye-Waller factor which accounts for thermal vibrations and possible static disorder (distribution of distances)

$$\sigma^2 = \sigma_{stat}^2 + \sigma_{vib}^2$$

static cofactor ← temperature dependence

low Debye-Waller factor ⇒ stronger EXAFS

$e^{-2r_j/\lambda}$ = damping term describing decay of the photoelectron wave due to inelastic scattering losses; λ is the mean free path of electron

r_j = distance of the j^{th} atom from the absorbing atom (absorber)

$\phi_j \equiv$ total phase shift experienced by the photoelectron

$$= \phi_a^l + \phi_b - l\pi$$

ϕ_a^l = phase shift due to absorber

ϕ_b = phase shift due to j^{th} scattering

and $l = 1$ for K edge; $l = 2$ for L_{II} and L_{III} edges

$L_I (^2S)$ $(^2P_{1/2})$ $(^2P_{3/2})$

$\chi(E)$ or $\chi(k)$ = oscillatory part of absorption in EXAFS region.

$$\chi(E) = \chi(k) = \frac{\mu(E) - \mu_0(E)}{\mu_0(E)}$$

where $\mu_0(E)$ = smooth "background" absorption coefficient.

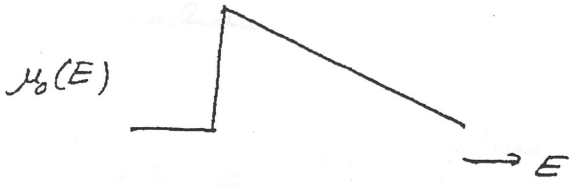

Recall $|k| = \left[\frac{2m_e(E-E_0)}{\hbar^2}\right]^{1/2}$

Because EXAFS signal is a very small part of the total signal, the above simple subtraction of a fitted curve from above the EXAFS region is not adequate. A Fourier filtering technique is typically used in conjunction with the subtraction. In this procedure, the large sawtooth-like function from the K-edge absorption is first removed by subtracting a straight line, obtained from the first and last data points of the EXAFS region. The energy points on the abscissa are then converted to momentum, or $|k|$ space. The resultant data are then transformed [redacted] into coordinate space, and back into $|k|$ space using various Fourier windows. This procedure eliminates unsuppressed contributions from remnants of the smoothly varying K-edge ([redacted] low frequency), EXAFS (intermediate frequencies), and random and instrumental noise (broad spectrum).

$$\phi(r) = \left(\frac{1}{2\pi}\right)^{1/2} \int_{k_{min}}^{k_{max}} \frac{\mu(E)^{(k)} - \mu_0(E)^{(k)}}{\mu_0(E)^{(k)}} e^{i2kr}\, dk$$

or

$$\phi'(r) = \left(\frac{1}{2\pi}\right)^{1/2} \int_{k_{min}}^{k_{max}} k^3 \cdot \frac{\mu(k) - \mu_0(k)}{\mu_0(k)} \cdot e^{i2kr}\, dk$$

to compensate for diminishing amplitudes at high $|k|$ values and to give more weight to data at high $|k|$ values.

$$\chi(k) = \left(\frac{1}{2\pi}\right)^{1/2} \int_{r_{min}}^{r_{max}} \left(\phi(r) \text{ or } \phi'(r)\right) e^{-i2kr}\, dr$$

Example

momentum to space

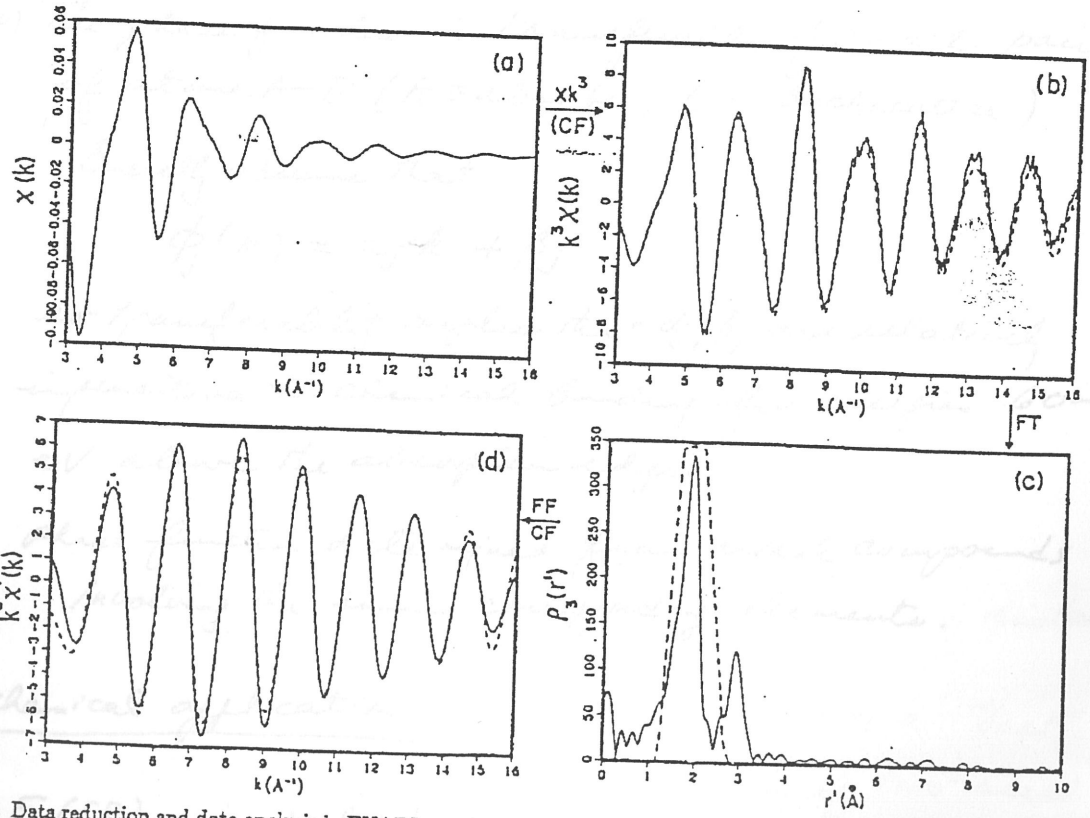

Data reduction and data analysis in EXAFS spectroscopy: (a) EXAFS spectrum $\chi(k)$ vs. k after background removal; (b) the solid curve is the weighted EXAFS spectrum $\chi(k)k^3$ vs. k after multiplying $\chi(k)$ by k^3. The dashed curve represents an attempt to fit the data with a two-distance model by curve-fitting (CF) technique; (c) Fourier transformation (FT) of the weighted EXAFS spectrum in momentum (k) space into the radial distribution function $\rho_3(r')$ vs. r' in distance space, r' is related to the true distance r by a "phase shift" $\alpha = r - r'$. The dashed curve is the window function used to filter the major peak in Fourier filtering (FF); (d) Fourier-filtered EXAFS spectrum $\chi'(k)k^3$ vs. k (solid curve) of the major peak in (c) after backtransforming into k space. The dashed curve attempts to fit the filtered data with a single-distance model.

Assumptions

(1) Short-range single-electron single-scattering, i.e., the single photoelectron ejected from an absorbing atom makes a single round trip from the absorber to the nearby scatterers lying within a short distance (~4Å) range from the absorber.

(2) EXAFS is a simple sum of waves due to various types of neighboring atoms (this implies that multiple scattering is relatively unimportant.

(3) The amplitude function is transferable for each type of backscatterer B

(4) The phase function is transferable for each pair of atoms A–B (A ≡ absorber; B ≡ backscatter)

Generally assume that

$$\phi_j(k) = \alpha_j k + \beta_j$$

so transferability implies that α_j, β_j are relatively insensitive to chemical bonding for energies 60–1000 eV above the absorption edges.

phase function determined from model compounds involving the same corresponding elements.

Biochemical application

$Fe(SR)_4$ in rubredoxin

and

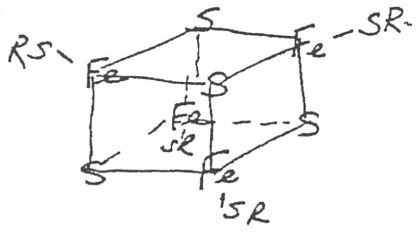

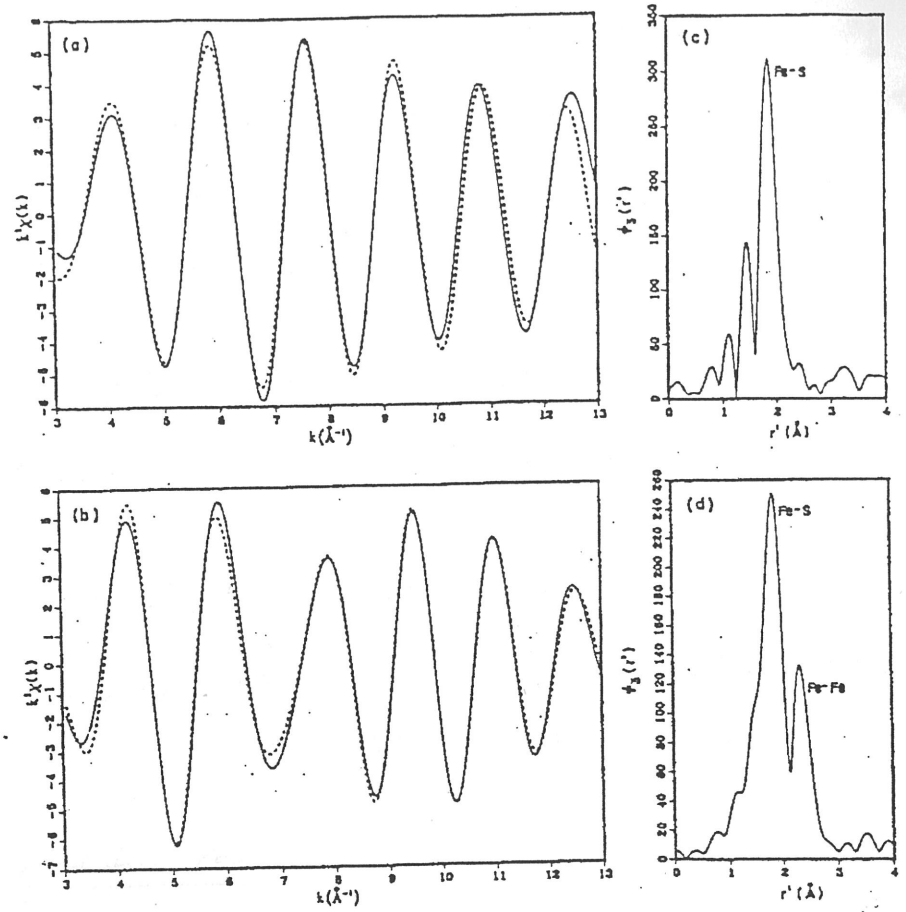

[redacted]. Fourier filtered (window: $r' = 0.9 \sim 3.5$ Å) EXAFS spectra (solid curves) and the theoretical fits (dashed curves) for (a) *single-shell* systems such as rubredoxin and (b) *two-shell* systems such as bacteria ferredoxin. In (a) a single term containing the average Fe–S distance was used whereas in (b) two terms containing the average Fe–S and Fe–Fe distances were used. The corresponding Fourier transforms of the $k^3\chi(k)$ vs. k data are shown in (c) and (d), respectively. The minor peaks to the left of the Fe–S peak are due to residual background and/or Fourier truncation.

Rubredoxin : monomeric $Fe(SR)_4$

Amplitude envelope varies smoothly with k indicative of a single shell with one type of distance.

Ferredoxin : tetranion oligomer exhibits a "beat" node at $k \sim 7 A^{\circ -1}$, characteristic of two-shell systems with two types of distances. The frequency at lower k region, which reflects the shorter Fe–S bonds, is lower than the frequency at higher k region, which is indicative of the longer Fe – Fe bonds

Fourier transforms of $\chi(k)k^3$ data reveal for the monomer one peak; but two peaks for the oligomers (also for the two Fe two S plant ferredoxin) $Fe_2S_2(SR)_4$. The major peak can be assigned to the Fe S bonds while the minor peak in each oligomer can be assigned to the Fe-Fe bond(s).

Note that $\phi(r)$ peaks at $r = R_j - \alpha_j$, so that to obtain R_j, α_j must be known

Debye Waller factor for pdredoxin: small

$\sigma_{stat} \Rightarrow$ Fe-S bonds are chemically equivalent to within 0.04Å.

Effect of reduction

Fe-S increases by 0.06Å upon reduction in pdredoxin, whereas lengthening of Fe-S and Fe-Fe bonds in oligomers upon reduction was quite small. ($\Delta r \leq 0.03$Å)

Synchrotron Radiation

To carry out the above experiments, need a source of tunable X-ray photons of high fluxes. The use of synchrotron radiation has met this need.

Origin of synchrotron radiation

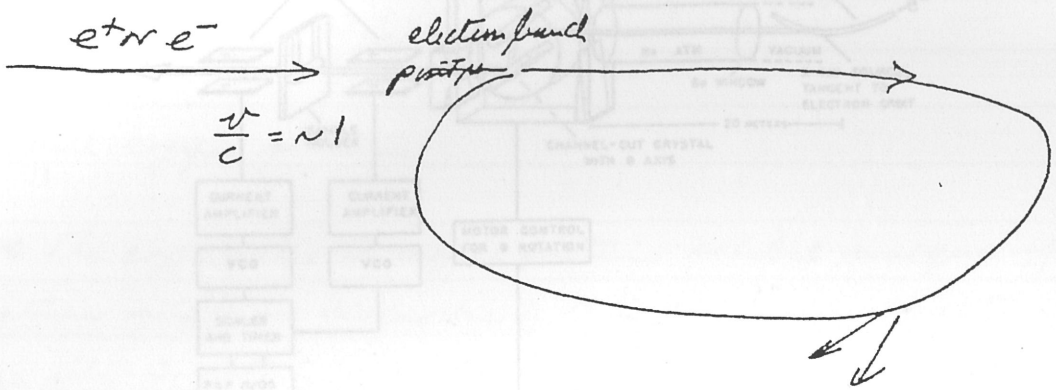

Position - Electron Accelerator Ring (Storage ring)

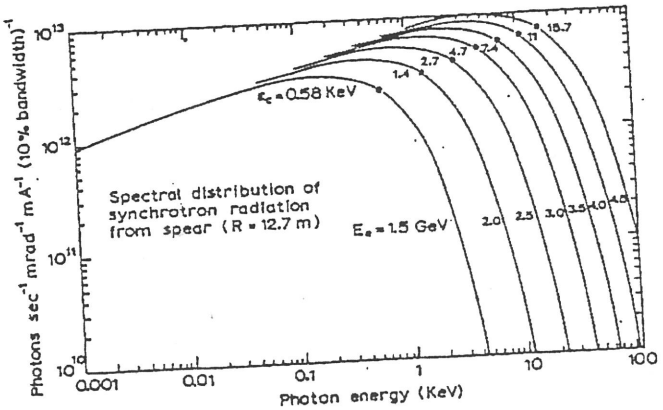

out-of date already

Nowadays ~ 10^8 photons sec^{-1} spread^{-1} mA^{-1}

or ~ 10^8 obtainable over conventionable X-ray sources.

Energy is not radiated continuously, but has a time structure: a single bunch of electrons orbits the storage ring 10^6 times/sec. and the entire group passes a point in the orbit in ~ 0.1 n sec. Radiation highly collimated and plane polarized in plane of electron orbit.

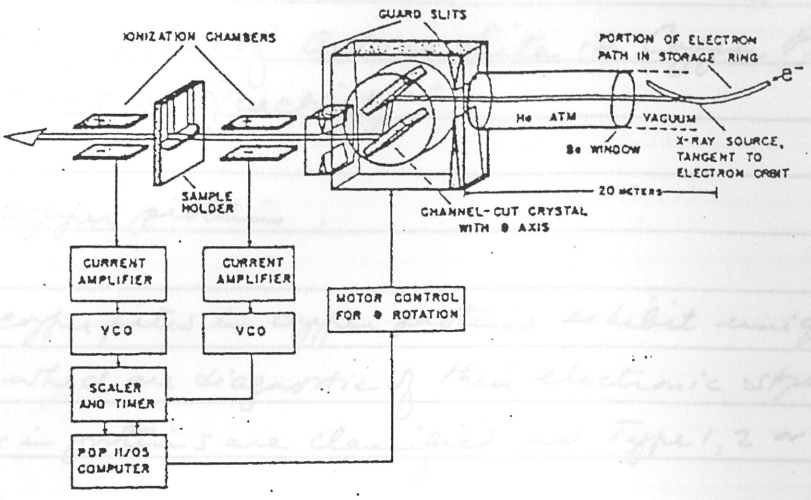

[redacted]. Diagram of the instrumentation for X-ray absorption spectroscopy. The drawing is not to proportion, as the storage ring is much larger than shown.

Reading Chem. Rev. (1992) 92, 521-542.

Lecture 2
February 2, 1993

E. I. Solomon, M. J. Baldwin, and M. D. Lowery.

"Electronic Structures of active Sites in Copper Proteins: Contributions to Reactivity"

Begin with copper proteins.

The copper sites in copper proteins exhibit unique spectral features which are diagnostic of their electronic structures. Copper sites in proteins are classified as Type 1, 2 or 3

Type 2 normal copper sites (tetragonal)

Type 1 blue site

Type 3 dinuclear copper site (coupled)

Type 2.

ex Cu, Zn SOD (1)

diamine oxidases (2)

dopamine β-monooxygenase (3) monooxygenase

galactose oxidase (4)

phenylalanine hydroxylase (5) monooxygenase

hemocyprein (6)

	MW	subunit # of Cu	
(1)	31 kDa, α_2,	2	$2O_2^{\cdot-} + 2H^+ \longrightarrow H_2O_2 + O_2$
(2)	160-200, α_2,	2	$R'CHNR_2 + O_2 + H_2O \longrightarrow R'CHO + HNR_2$
			cofactor 6-hydroxydopa (TOPA)
(3)	290, α_4	4 or 8	dopamine + ascorbate + O_2
			$\longrightarrow$ noradrenaline + dehydroascorbate
(4)	32 kDa	1	$RCH_2OH + O_2 \xrightarrow{+H_2O} RCHO + H_2O_2$

(5) 68kDa, −1 phenylalanine + O_2 → tyrosine + H_2O (2)

cofactor tetrahydropterin

(6) 9kDa −1 adrenaline / adrenochrome equilibrium

Model cupric complex

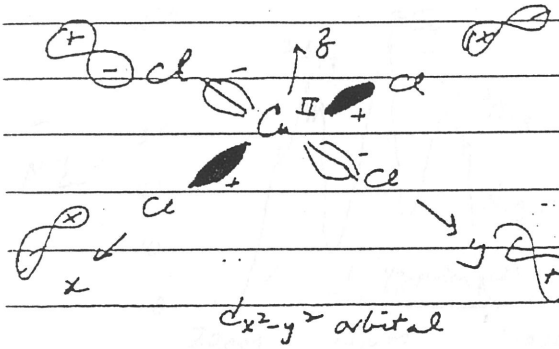

D_{4h} square planar $CuCl_4^{2-}$

z ⊥ tetragonal plane
equatorial plane

$d_{x^2-y^2}$ orbital

Ligand-field splitting of d orbitals in D_{4h} symmetry

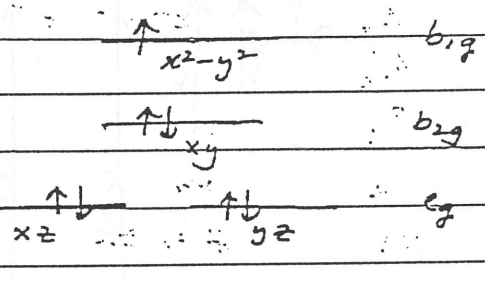

if start with O_h $(t_{2g})^6(e_g)^3$ gives ^2E_g ground state for Cu^{2+} complex but Jahn-Teller distortion leads to tetragonal distortion along z axis resulting in 4 tightly bound ligands

$^2B_{1g}$ ground state

According to SCF X_α scattered wave calculations, Ground state has 61% Cu(II) $d_{x^2-y^2}$ character with rest of the wavefunction made up of 9% contribution each from the 4 3p orbitals of the Chloride ligands

$$\psi_{MO} = a\, d^{Cu}_{x^2-y^2} + b\left(3p_{\sigma_1}^{Cl} + 3p_{\sigma_3}^{Cl} - 3p_{\sigma_2}^{Cl} - 3p_{\sigma_4}^{Cl}\right)$$

with $a^2 + 4b^2 = 1$, $a^2 = \underline{61\%}$

Excited state (low lying) d-d transitions

note that sign of ψ determined by Yeste

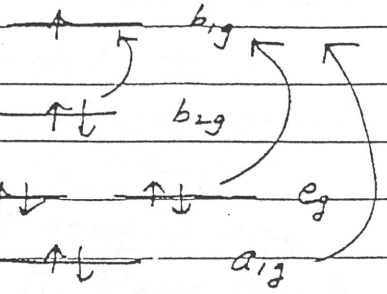

$\rightarrow {}^2B_{2g}$

$\rightarrow {}^2E_g$

$\rightarrow {}^2A_{1g}$ parity

$\frac{\nu}{c} \cong 15{,}400\ cm^{-1}$

$\frac{c}{\nu} \cong 6.5 \times 10^{-5}\ cm$

$\cong 6.5 \times 10^{-5} \times 10^7\ nm$

$\cong 670\ nm$

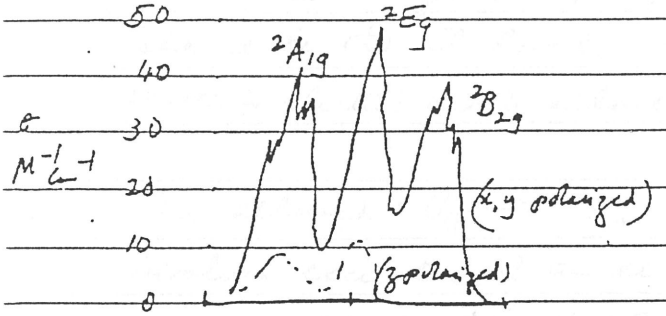

d-d transitions or ligand field transitions

Laporté (parity) forbidden

"allowed" or possible through coupling with odd parity vibrations.

$\epsilon < 50\ M^{-1}cm^{-1}$

550-800 nm

parity.

Excited States (Ligand to Metal charge transfer LMCT)

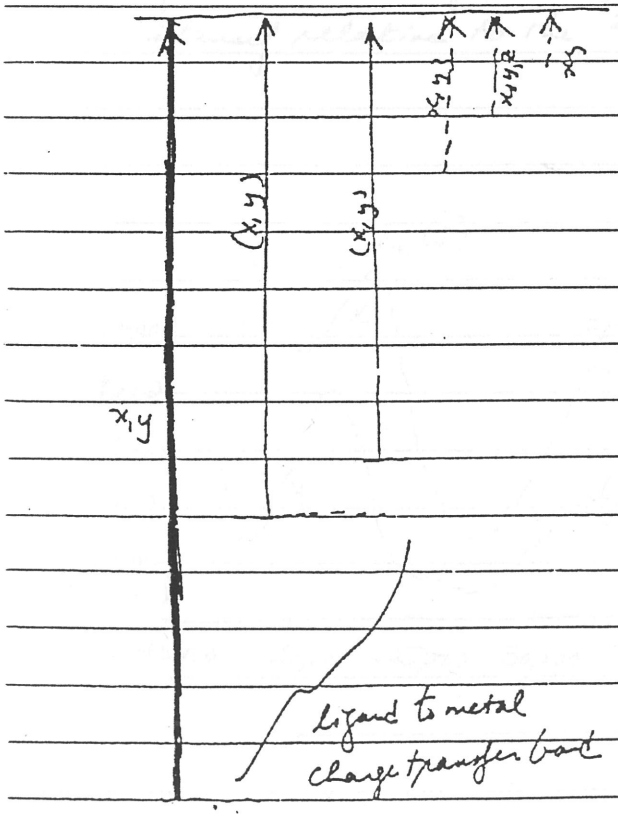

$\epsilon \sim 5000-10{,}000\ M^{-1}cm^{-1}$

optical transition from a filled chloride centered level to the half-filled copper centered $d_{x^2-y^2}$ orbital

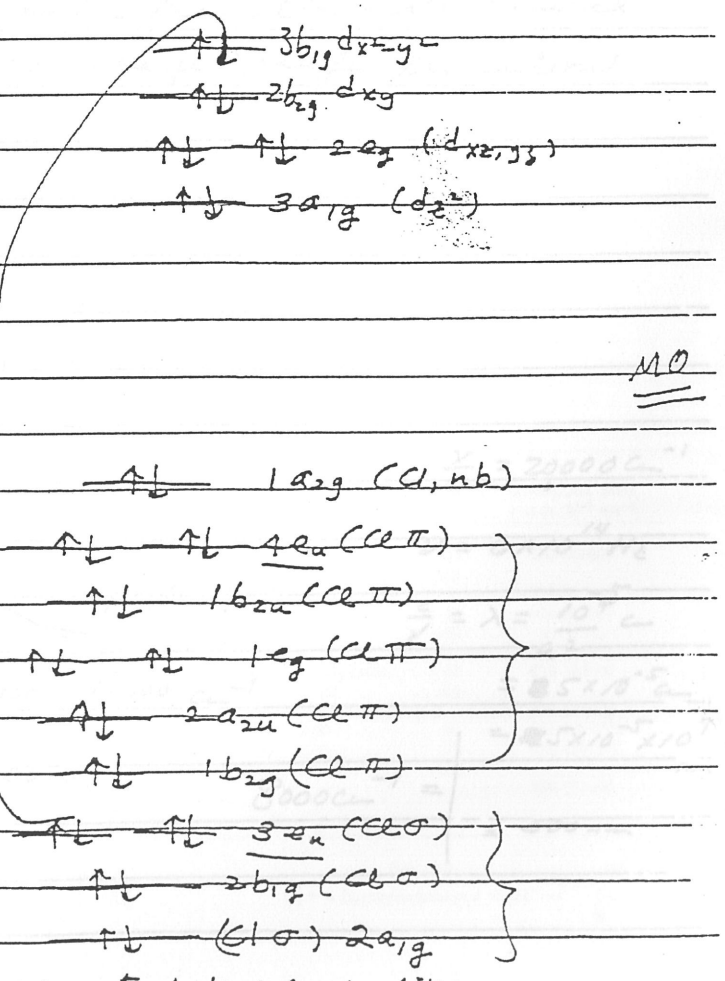

Each Chloride has 3 valence 3p orbitals, which split in energy due to bonding interactions with the metal ion. Those involved in σ bonding are deepest in energy due to greater ligand-metal overlap. The overlap of the donor and acceptor orbitals involved in the charge transfer process also governs the intensity of a charge transfer transition, and since the half-occupied $d_{x^2-y^2}$ level has only σ-overlap with the ligands, the charge transfer transition of greatest intensity should be the $Cl\ p\pi - b_{1u} \longrightarrow Cu\ d_{x^2-y^2}$ ($^2B_{1g} \rightarrow {}^2E_u(\sigma)$) which is electric dipole allowed & x, y polarized.

The allowed $^2B_{1g} \rightarrow {}^2E_u(\pi)$ charge-transfer transition involves excitation of an electron from a π-bonding ligand valence orbital into the $Cu_{d_{x^2-y^2}}$ level and thus should have no intensity. However, it interacts configurationally with the $^2E_u(\sigma)$ transition, leading to the appearance of a lower energy charge transfer transition with reduced intensity relative to the $^2E_u(\sigma)$ charge transfer transition

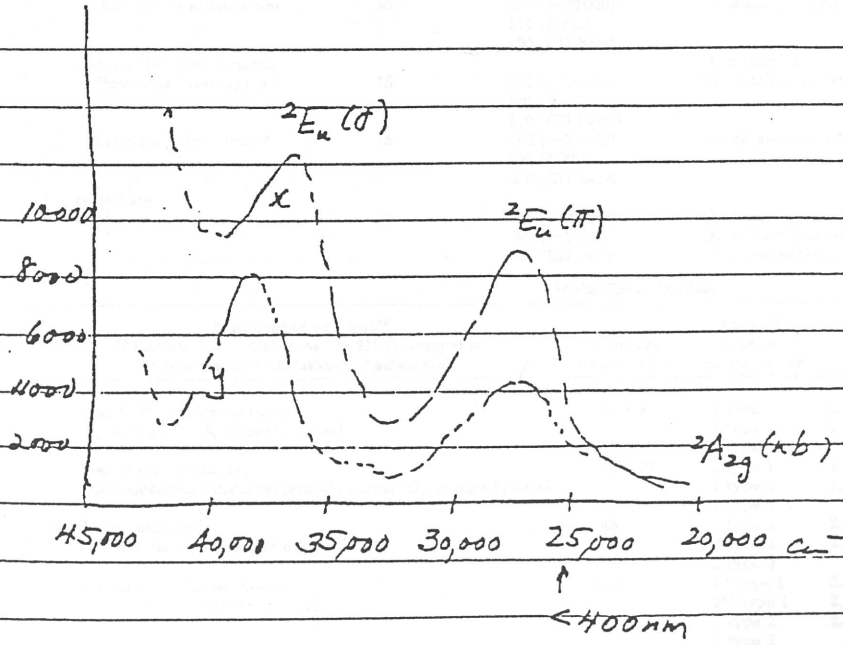

$\frac{\nu}{c} = 20000\,cm^{-1}$

$\nu = 6\times10^{14}\,Hz$

$\frac{c}{\nu} = \lambda = \frac{10^{-5}}{0.2}\,cm$

$= .5\times10^{-5}\,cm$

$8000\,cm^{-1} = \frac{= .5\times10^{-5}\times10^{7}\,nm}{= 500\,nm}$

TABLE I. Copper Proteins[1]

Normal Copper Enzymes

normal copper enzymes	molecular weight (in kDa), subunits, no. of Cu	function	cofactor[1]	ref
copper–zinc superoxide dismutase[a]	31, α_2, 2	$2O_2^- + 2H^+ \rightarrow H_2O_2 + O_2$		a
diamine oxidases	160–200, α_2, 2	$R'CHNR_2 + O_2 + H_2O \rightarrow R'CHO + HNR_2$	6-hydroxydopa (TOPA)	b
dopamine β monooxygenase	290, α_4, 4 or 8	dopamine + ascorbate + O_2 → noradrenaline + dehydroascorbate + H_2O		c
galactose oxidase[a]	32, –, 1	$RCH_2OH + O_2 \rightarrow RCHO + H_2O_2$	tyrosine radical	d
phenylalanine hydroxylase	68, –, 1	phenylalanine + O_2 → tyrosine + H_2O	tetrahydropterin	e
neurocuprein	9, –, 1	adrenaline/adrenochrome equilibrium?		f

Blue Copper Proteins

blue copper proteins[g] [function: electron transfer]	molecule weight, Da	redox potential, mV (pH)	blue band energy, nm (ϵ, M^{-1} cm^{-1})	EPR: $A \times 10^{-4}$ cm^{-1} $g_\parallel$	$g_\perp$ g_y	$g_\perp$ g_x	$A_\parallel$ A_z	$A_\perp$ A_y	$A_\perp$ A_x	ref
plastocyanin[a,i]	10 500	+370 (7.0)	597 (4500)	2.226	2.059	2.042	63			h
azurins										i
Alcaligenes denitrificans[a]	14 000	+276 (7.0)	619 (5100)	2.255	2.059		60			22
Alcaligenes faecalis S-6[a]	14 000	+266 (7.0)	593							21b
Pseudomonas aeruginosa[a]	14 600	+308 (7.0)	631 (3800)	2.260	2.052		60			
Pseudomonas denitrificans[a]	14 600			2.260	2.055		60			
stellacyanin	20 000	+184 (7.1)	609 (3400)	2.287	2.077	2.025	37	28	54	j
amicyanin[j]	13 800	+261 (7.0)	596 (3950)	2.239	2.046		59	36		k
auracyanin	12 800	+240 (8.0)	596 (2900)	2.210	2.062	2.018	47	12	62	l
cucumber basic blue[a]	10 100	+317 (7.0)	597 (4500)	2.207	2.08	2.02	55	10	60	m
mavicyanin	18 000	+285 (7.0)	600 (5000)	2.287	2.077	2.025	37	28	54	n
rusticyanin	16 500	+680 (2.0)	597 (2240)	2.229	2.064	2.019	47	19	61	o
umecyanin	14 600	+283 (7.0)	610 (3400)	2.317	2.05		38			p

Normal + Blue Copper Enzymes

normal + blue copper enzymes[g] [function: $NO_2^- \rightarrow NO$]	molecular weight (in kDa), subunits, no. of Cu	blue band energy, nm (ϵ, M^{-1} cm^{-1})	EPR parameters $g_\parallel$	EPR parameters $A_\parallel$ ($\times 10^{-4}$ cm^{-1})	ref
nitrite reductase					
Achromobacter cycloclastes[a]	69, α_2, 6	590 (2000)	type 1 2.195 type 2 2.262	type 1 73 type 2 175	q

Binuclear Copper Proteins

binuclear copper proteins[k]	molecular weight, kDa, per Cu_2 site[r]	O_2^{2-}—Cu CT bands,[s] nm (ϵ, M^{-1} cm^{-1})	function	ref
molluscan hemocyanins			O_2 transport	t, u
Busycon canaliculatum	50	350 (~20 000) 570 (1000) 480 (CD band)	(catalase activity: $2H_2O_2 \rightarrow 2H_2O + O_2$)	
arthropodan hemocyanins			O_2 transport	39, 56, t, u
Panulirus interruptus[a]	75	335 (~20 000) 580 (800) 510 (CD band)	(no catalase activity)	
Limulus polyphemus[a]	75	340 (~20 000) 590 (1000) 500 (CD band)	(no catalase activity)	
tyrosinase				62, 63, v
Neurospora crassa	42	345 (~20 000) 590 (~1000) 520 (CD band)	$O_2 + 2H^+ +$ monophenol → o-diphenol + H_2O $O_2 + 2$ o-diphenol → 2 o-quinone + $2H_2O$ (catalase activity)	

Multicopper Oxidases

multicopper oxidases[26] [function: $O_2 + 4H^+ + 4e^- \rightarrow 2H_2O$ coupled to 4 one-electron oxidations of substrate]	molecular weight, kDa	no. and type of copper center	EPR parameters $g_\parallel$	EPR parameters $g_\perp$	EPR parameters $A_\parallel \times 10^{-4}$, cm^{-1}	absorption band, nm (ϵ, M^{-1} cm^{-1})
laccase						
Fungal: *Polyspora versicolor* (p-diphenol: O_2 oxidoreductase)	60–90	1 type 1	2.19	2.03	90	610 (4900)
		1 type 2	2.24	2.04	194	
		1 type 3				330 (2700)
Tree: *Rhus vernicifera* (monophenol, dihydroxyphenylalanine: O_2 oxidoreductase)	110–140	1 type 1	2.23	2.05	43	615 (5700)
		1 type 2	2.24	2.05	200	
		1 type 3				330 (2800)
ascorbate oxidase[a,24] (L-ascorbate: O_2 oxidoreductase)	145	2 type 1	2.227	2.058, 2.036	58	610 (4800)
		2 type 2	2.242	2.053	199	
		2 type 3				330 (2000)
ceruloplasmin or ferroxidase I (iron(II): O_2 oxidoreductase)	130	1st type 1	2.215	2.06	92	610 (10 000)
		2nd type 1	2.206	2.05	72	610 (10 000)
		1 type 2	2.247	2.06	189	
		1 type 3				330 (3300)

Cu_A-Containing Enzymes

Cu_A-containing enzymes	molecular weight (in kDa), subunits	metal centers	function	ref
cytochrome c oxidase	170, 12	hemes (Fe_a and Fe_{a3}), Cu_A, Cu_B	$O_2 +$ 4 ferrocytochrome c + $4H^+ \rightarrow$	2b, w

TABLE I (Continued)

Cu_A-containing enzymes	molecular weight (in kDa), subunits	metal centers	function	ref
		Cu_A-Containing Enzymes		
		(Cu_A antiferromagnetically coupled to Fe_A)	$2H_2O + 4$ ferricytochrome c	
nitrous oxidase reductase			$N_2O + 2e^- + 2H^+ \rightarrow N_2 + H_2O$	z
Pseudomonas stutzeri	140, α_2	2 Cu_A, 6 other Cu atoms		
Pseudomonas aeruginosa	73, α_2	4 Cu atoms/molecule		

[i] In addition to the proteins listed in Table I other proteins which have been suggested to require copper for activity are listed in footnote *y*. [j] A high-resolution x-ray crystal structure has been reported. [k] Preliminary crystallographic data have been reported. See references for details. [l] A NMR structure has been reported. [m](1) Valentine, J. S.; Pantoliano, M. W. In *Copper Proteins*; Spiro, T. G., Ed.; Wiley-Interscience: New York, 1981; pp 291–358. (2) Strothkamp, K. G.; Lippard, S. J. *Acc. Chem. Res.* **1982**, *15*, 318–326. (3) Fee, J. A.; Peisach, J.; Mims, W. B. *J. Biol. Chem.* 1981, *256*, 1910–1914. (4) Fieldan, E. M.; Rotilio, G. In *Copper Proteins and Copper Enzymes*; Lontie, R., Ed.; CRC Press: Boca Raton, FL, 1984; Vol. II, Chapter 2. (5) For a 2.0-Å X-ray crystal structure of bovine erythrocyte Cu,Zn SOD, see: Tainar, J. A.; Getzoff, E. D.; Beem, K. M.; Richardson, J. S.; Richardson, D. C. *J. Mol. Biol.* 1982, *160*, 181–217. Tainar, J. A.; Getzoff, E. D.; Richardson, J. S.; Richardson, D. C. *Nature* 1983, *306*, 284–287. (6) For a 2.5-Å resolution structure of yeast SOD, see: Djinovic, K.; Gatti, G.; Coda, A.; Antolini, L.; Pelosi, G.; Desideri, A.; Falconi, M.; Marmocchi, F.; Rotilio, G.; Bolognesi, M. *Acta Crystallogr.* 1991, *B47*, 918–927. [n](1) Dooley, D. M. *Life Chem. Rep.* 1987, *5*, 91–154. (2) *Structure and Functions of Amine Oxidases*; Mondovi, B., Ed.; CRC Press: Boca Raton, FL, 1985. (3) Knowles, P. F.; Yadav, K. D. S. In *Copper Proteins and Copper Enzymes*; Lontie, R., Ed.; CRC Press: Boca Raton, FL, 1984; Vol. II, Chapter 4. [o](1) Ljones, T.; Skotland, T. In *Copper Proteins and Copper Enzymes*; Lontie, R., Ed.; CRC Press: Boca Raton, FL, 1984; Vol. II, Chapter 5. (2) Villafranca, J. J. In *Copper Proteins*; Spiro, T. G., Ed.; Wiley-Interscience: New York, 1981; Chapter 7. [p](1) Ettinger, M. J.; Kosman, D. J. In *Copper Proteins*; Spiro, T. G., Ed.; Wiley-Interscience: New York, 1981; Chaptar 8. (2) See reference 1c for X-ray structure. [q]Benkovic, S.; Wallick, D.; Bloom, L.; Gaffney, B. J.; Domanico, P.; Dix, T.; Pamber, S. *Biochem. Soc. Trans.* 1985, *13*, 436–438. See reference 1a for cofactor. [r](1) Mikaelyan, M. V.; Nalbandyan, R. M. *Neurochem. Int.* 1988, *13*, 435–438. (2) Mikaelyan, M. V.; Nalbandyan, R. M. *Neurochem. Int.* 1985, *7*, 1073–1078. (3) Sharoyan, S. G.; Shaljian, A. A.; Nalbandyan, R. M.; Buniatian, H. C. H. *Biochim. Biophys. Acta* 1977, *493*, 478–487. [s]For recent reviews see: (1) Adman, E. T. In *Advances in Protein Chemistry*; Anfinsen, C. B., Edsall, J. T., Richards, F. M.; Eisenberg, D. S., Eds.; Academic Press: San Diego, 1991; Vol. 42, pp 145–198. (2) Sykes, A. G. *Struct. Bond.* 1991, *75*, 175–224. (3) Sykes, A. G. *Adv. Inorg. Chem.* 1991, *36*, 377–408. (4) Farver, O.; Pecht, I. *Coord. Chem. Rev.* 1989, *94*, 17–45. (5) Gray, H. B. *Chem. Soc. Rev.* 1986, *15*, 17–30. (6) Lappin, A. G. In *Metal Ions in Biological Systems*; Sigel, H., Ed.; Dekker: New York, 1981; Vol. 13; Chapter 2. (7) Adman, E. T. *Top. Mol. Struct. Biol.* 1985, *6*, 1–42. [t]Data shown here are for spinach plastocyanin (see *g*). For the NMR-determined structure of french bean plastocyanin see: Moore, J. M.; Lepre, C. A.; Gippert, G. P.; Chazin, W. J.; Case, D. A.; Wright, P. E. *J. Mol. Biol.* 1991, *221*, 533–555. X-ray structures exist for poplar plastocyanin: see ref 20 and Guss, J. M.; Freeman, H. C. *J. Mol. Biol.* 1983, *169*, 521–563. For Cu(I) poplar plastocyanin, see: Guss, J. M.; Harrowell, P. R.; Murata, M.; Norris, V. A.; Freeman, H. C. *J. Mol. Biol.* 1986, *192*, 361–387. [u]For the X-ray structure for *A. denitrificans*, see: ref 22. For *A. faecalis* S-6, see: ref 21b. For *P. aeruginosa*, see: Nar, H.; Messerschmidt, A.; Huber, R.; van de Kamp, M.; Canters, G. W. *J. Mol. Biol.* 1991, *221*, 765–772. For *P. denitrificans*, see: ref 22. [v]Peisach, J.; Levine, W. G.; Blumberg, W. E. *J. Biol. Chem.* 1967, *242*, 2847–2858. [w]The data shown are for *Thiobacillus versutus*, see: (1) Houwelingen, T. V.; Canters, G. W.; Stobbelaar, G.; Duine, J. A.; Frank, J.; Tsugita, A. *Eur. J. Biochem.* 1985, *153*, 75–80. (2) Lommen, A.; Canters, G. W.; van Beeumen, J. *Eur. J. Biochem.* 1988, *176*, 213–223. (3) Lommen, A.; Canters, G. W. *J. Biol. Chem.* 1990, *265*, 2768–2774. (4) A preliminary X-ray structure has been reported: Petratos, K.; Dauter, Z.; Wilson, K. S.; Lommen, A.; van Beeumen, J.; Cantera, G. W. *J. Mol. Biol.* 1988, *199*, 545–546. Additional amicyanin include organism 4025: Lawton, S. A.; Anthony, C. *Biochem. J.* 1985, *228*, 719–728. *Paracoccus denitrificans*: (1) Husain, M.; Davidson, V. L. *J. Biol. Chem.* 1985, *260*, 14626–14629. (2) Husian, M.; Davidson, V. L.; Smith, A. J. *Biochemistry* 1986, *25*, 2431–2436. (3) Sharma, K. D.; Loehr, T.; Sanders-Loehr, J.; Husain, M.; Davidson, V. L. *J. Biol. Chem.* 1988, *263*, 3303–3306. *Pseudomonas* AM1: (1) Tobari, J.; Harada, Y. *Biochem. Biophys. Res. Commun.* 1981, *101*, 502–508. (2) Ambler, R. P.; Tobari, J. *Biochem. J.* 1985, *232*, 451–457. *Methylomonas* J: Ambler, R. P.; Tobari, J. *Biochem. J.* 1989, *261*, 495–499. [x]Trost, J. T.; McManus, J. D.; Freeman, J. C.; Ramakrishna, B. L.; Blankenship, R. E. *Biochemistry* 1988, *27*, 7858–7863. [y](1) Colman, P. M.; Freeman, H. C.; Guss, J. M.; Murata, M.; Norris, V. A.; Ramshaw, J. A. M.; Venkatappa, M. P.; Vickery, L. E. *J. Mol. Biol.* 1977, *112*, 649–650. (2) Murata, M.; Begg, G. S.; Lambrou, F.; Leslie, B.; Simpson, R. J.; Freeman, H. C.; Morgan, F. J. *Proc. Natl. Acad. Sci. U.S.A.* 1982, *79*, 6434–6437.. (3) A 3.0-Å resolution X-ray structure has been reported, see: Guss, J. M.; Merritt, E. A.; Phizackerley, R. P.; Hedman, B.; Murata, M.; Hodgson, K. O.; Freeman, H. C. *Science* 1988, *241*, 806–811. [z]Marchesini, A.; Minelli, M.; Markle, H.; Kroneck, P. M. H. *Eur. J. Biochem.* 1979, *101*, 77–84. [aa](1) Cobley, J. G.; Haddock, B. A. *FEBS Lett.* 1975, *60*, 29–33. (2) Cox, J. D.; Boxer, D. H. *Biochem. J.* 1978, *174*, 497–502. (3) Ingledew, W. J.; Cobley, J. C. *Biochim. Biophys. Acta* 1980, *590*, 141–158. (4) Ingledew, W. J. *Biochim. Biophys. Acta* 1982, *683*, 89–117. (5) Cox, J. C.; Aasa, R.; Malmström, B. G. *FEBS Lett.* 1978, *93*, 157–160. [ab]Paul, K. G.; Stigbrand, T. *Biochim. Biophys. Acta* 1970, *221*, 255–263. [ac]Data shown are for *Achromobacter cycloclastes*. For a 2.3-Å X-ray crystal structure, see: (1) Godden, J. W.; Turley, S.; Teller, D. C.; Adman, E. T.; Liu, M. Y.; Payne, W. J.; LeGall, J. *Science* 1991, *253*, 438–442. (2) Fanderson, F. F.; Kumar, S.; Adman, E. T.; Liu, M. Y.; Payne, W. J.; LeGall, J. *Biochemistry* 1991, *30*, 7180–7185. (3) Suzuki, S.; Yoshimura, T.; Kohzuma, T.; Shidara, S.; Masuko, M.; Sakurai, T.; Iwasaki, H. *Biochem. Biophys. Res. Commun.* 1989, *164*, 1366–1372. (4) Hulse, C. L.; Averill, B. A.; Tiedje, J. M. *J. Am. Chem. Soc.* 1989, *111*, 2322–2323. (5) Dooley, D. M.; Moog, R. S.; Liu, M. Y.; Payne, W. J.; LeGall, J. *J. Biol. Chem.* 1988, *263*, 14625–14628. (6) Kashem, M. A.; Dumford, H. B.; Liu, M. Y.; Payne, W. J.; LeGall, J. *Biochem. Biophys. Res. Commun.* 1987, *145*, 563–568. (7) Liu, M. Y.; Liu, M. C.; Payne, W. J.; LeGall, J. *J. Bacteriol.* 1986, *166*, 604–608. (8) Iwasaki, H.; Noji, S.; Shidara, S. *J. Biochem. (Tokyo)* 1975, *78*, 355–361. *Pseudomonas aureofaciens*: Zumft, W. G.; Gotzmann, D. J.; Kroneck, P. M. H. *Eur. J. Biochem.* 1987, *168*, 301–307. *Pseudomonas aeruginosa*: Karapetian, A. V.; Kamalian, M. G.; Malbandyan, R. M. *FEBS Lett.* 1986, *203*, 131–134. *Nitrosomonas europaea*: (1) Miller, D. J.; Nicholas, D. J. D. *J. Gen. Microbiol.* 1985, *131*, 2851–2854. (2) Miller, D. J.; Wood, P. M. *J. Gen. Microbiol.* 1983, *129*, 1645–50. From *Alcaligenes* sp. NCIB 11015: (1) Sakurai, T.; Suzuki, S.; Nakahara, A.; Masuko, M.; Iwasaki, H. *Chem. Lett.* 1985, *9*, 1297–1300. (2) Masuko, M.; Iwasaki, H.; Sakurai, T.; Suzuki, S.; Nakahara, A. *J. Biochem. (Tokyo)* 1984, *96*, 447–454. *Rhodopseudomonas sphaeroides* forma sp. *denitrificans*: Michalski, W. P.; Nicholas, D. J. D. *Biochim. Biophys. Acta* 1985, *828*, 130–7. From *Alcaligenes* sp: Sano, M.; Matsubara, T. *Chem. Lett.* 1984, *12*, 2121–2124. *Alcaligenes faecalis* S6: (1) Kakutani, T.; Watanabe, H.; Arima, K.; Beppu, T. *J. Biochem. (Tokyo)* 1981, *89*, 463–472. (2) Kakutani, T.; Watanabe, H.; Arima, K.; Beppu, T. *J. Biochem. (Tokyo)* 1981, *89*, 453–461. A preliminary X-ray structure has been reported: Petratos, K.; Beppu, T.; Banner, D. W.; Tsernoglou, D. *J. Mol. Biol.* 1986, *190*, 135. [ad]Molecular weights are given per binuclear site. For molluscan hemocyanins, there are approximately 20 subunits per molecule, each containing 8 oxygen-binding domains of the given molecular weight. Arthropodan hemocyanins have dissociable subunits of the given molecular weight, each containing a single oxygen-binding site, with as many as 48 subunits per molecule assembled as hexamers, depending on the species. Tyrosinase has a single active site per molecule. [ae]These spectral features are for the oxy form of the protein, which is the resting form for the hemocyanins. The resting form of tyrosinase is the met form. [af]Nickerson, K. W.; van Holde, K. E. *Comp. Biochem. Physiol.* 1971, *39B*, 855–872. [ag]Himmelwright, R. S.; Eickman, N. C.; LuBien, C. D.; Solomon, E. I. *J. Am. Chem. Soc.* 1980, *102*, 5378–5388. [ah]Lerch, K. *FEBS Lett.* 1978, *89*, 157–160. [ai](1) Kroneck, P. M.; Antholine, W. E.; Kastrau, D. H. W.; Buse, G.; Steffens, G. C. M.; Zumft, W. G. *FEBS Lett.* 1990, *268*, 274–276. (2) Larsen, R. W.; Ondrias, M. R.; Copeland, R. A.; Li, P. M.; Chan, S. I. *Biochemistry* 1989, *28*, 6418–6422. [aj]References for *Pseudomonas stutzeri*: (1) Dooley, D. M.; McGuirl, M. A.; Rosenzweig, A. C.; Landin, J. A.; Scott, R. A.; Zumft, W. G.; Devlin, F.; Stephens, P. J. *Inorg. Chem.* 1991, *30*, 3006–3011. (2) Zumft, W. G.; Viebrock-Sambale, A.; Braun, C. *Eur. J. Biochem.* 1990, *192*, 591–599. (3) Riester, J.; Zumft, W. G.; Kroneck, P. M. H. *Eur. J. Biochem.* 1989, *178*, 751–762. (4) Dooley, D. M.; Moog, R. S.; Zumft, W. G. *J. Am. Chem. Soc.* 1987, *109*, 6730–6735. (5) Scott, R. A.; Zumft, W. G.; Coyle, C. L.; Dooley, D. M. *Proc. Natl. Acad. Sci. U.S.A.* 1989, *86*, 4082–4086. (6) Kroneck, P. M. H.; Antholine, W. A.; Riester, J.; Zumft, W. G. *FEBS Lett.* 1988, *242*, 70–74. (7) Coyle, C. L.; Zumft, W. G.; Kroneck, P. M. H. *Life Chem. Rep.* 1987, *5*, 289–303. (8) Dooley, D. M.; Moog, R. S.; Zumft, W. G. *J. Am. Chem. Soc.* 1987, *109*, 6730–6735. (9) Zumft, W. G.; Matsubara, T. *FEBS Lett.* 1982, *148*, 107–112. (10) Coyle, C. L.; Zumft, W. G.; Kroneck, P. M. H.; Körner, H.; Jakob, W. *Eur. J. Biochem.* 1985, *153*, 459–467. *Alcaligenes* sp: Matsubara, T.; Sano, M. *Chem. Lett.* 1985, *7*, 1053–1056. *Paracoccus denitrificans*: Snyder, S. W.; Hollocher, T. C. *J. Biol. Chem.* 1987, *262*, 6515–6525. *Pseudomonas aeruginosa*: (1) SooHoo, C. K.; Hollocher, T. C.; Kolodziej, A. F.; Orme-Johnson, W. H.; Bunker, G. *J. Biol. Chem.* 1991, *266*, 2210–2218. (2) SooHoo, C. K.; Hollocher, T. C. *J. Biol. Chem.* 1991, *266*, 2203–2209. *Achromobacter cycloclastes*: (1) Hulse, C. L.; Averill, B. A. *Biochem. Biophys. Res. Commun.* 1990, *166*, 729–735. [ak](1) Bilirubin oxidase: Gotoh, Y.; Kondo, Y.; Kaji, J.; Takeda, A.; Samejima, T. *J. Biochem.* 1989, *106*, 621–628. (2) Glycerol oxidase: Uwajima, T.; Shimizu, Y.; Terada, O. *J. Biol. Chem.* 1984, *259*, 2748–2753. (3) Methane monooxygenase: (a) Shiemke, A. K.; DiSpirito, A. A.; Lidstrom, M. E.; Chan, S. I. *J. Inorg. Biochem.* 1991, *43*, 191. (b) Tonge, G. M.; Harrison, D. E. F., Higgins, I. J. *Biochem. J.* 1977, *161*, 333–344. (4) Peptidyl-glycine α-amidating monooxygenase (PAM): Eipper, B. A.; Mains, R. E.; Glembotski, C. C. *Proc. Natl. Acad. Sci. U.S.A.* 1983, *80*, 5144–5148. (5) Ferroxidase II: Garnier, A.; Tosi, L.; Steinbuch, M. *Biochem. Biophys. Res. Commun.* 1981, *98*, 66–71. (6) Uridine nucleosidase: Magni, G.; Natalini, P.; Ruggieri, S.; Vita, A. *Biochem. Biophys. Res. Commun.* 1976, *69*, 724–730. (7) Quercetinase: Oka, T.; Simpson, F. J. *Biochem. Biophys. Res. Commun.* 1971, *43*, 1–5. (8) Phenylethylamine oxidase: Shimizu, E.; Ichise, H.; Yorifuji, T. *Agric. Biol. Chem.* 1990, *54*, 851–853.

Blue Copper Site

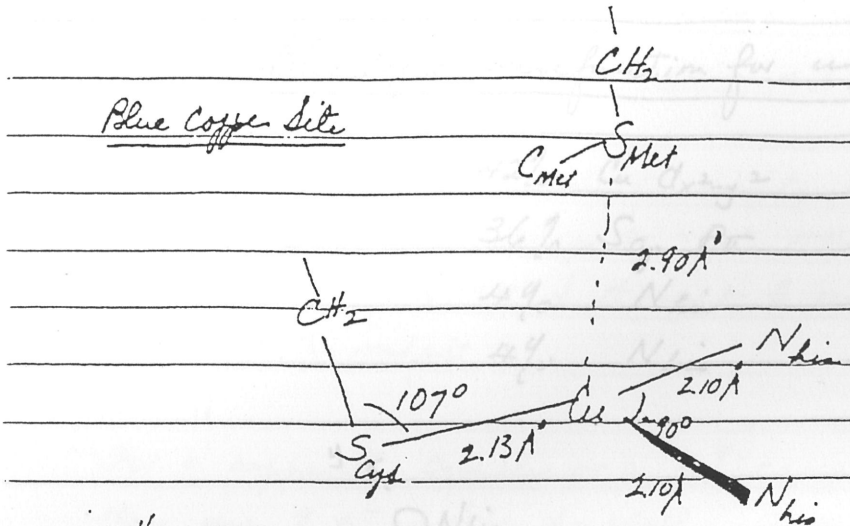

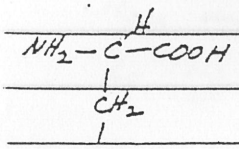

cysteine

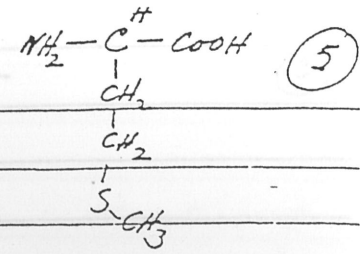

methionine

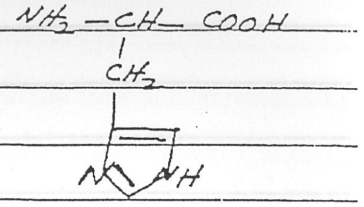

Histidine

From

Hans Freeman et al

Nature (1978) 272, 319-324.

Cu d orbitals

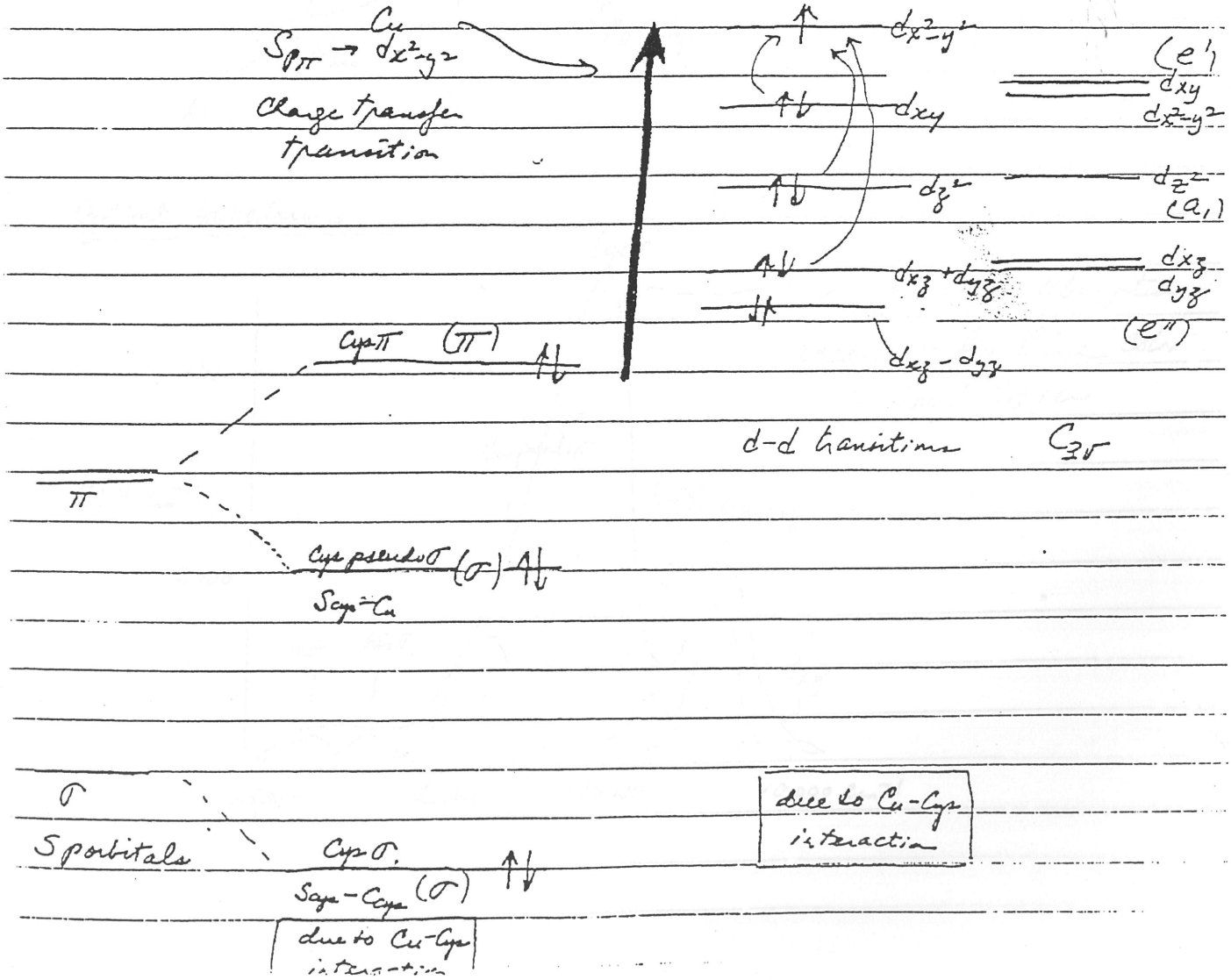

Blue copper wavefunction for unpaired e⁻

42% Cu $d_{x^2-y^2}$

36% S_{Cys} p_π

4% N_{his}

4% N_{his}

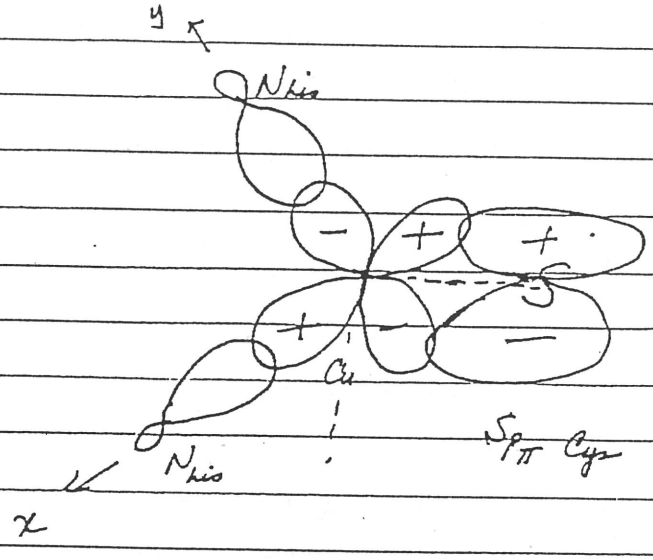

Optical Spectrum

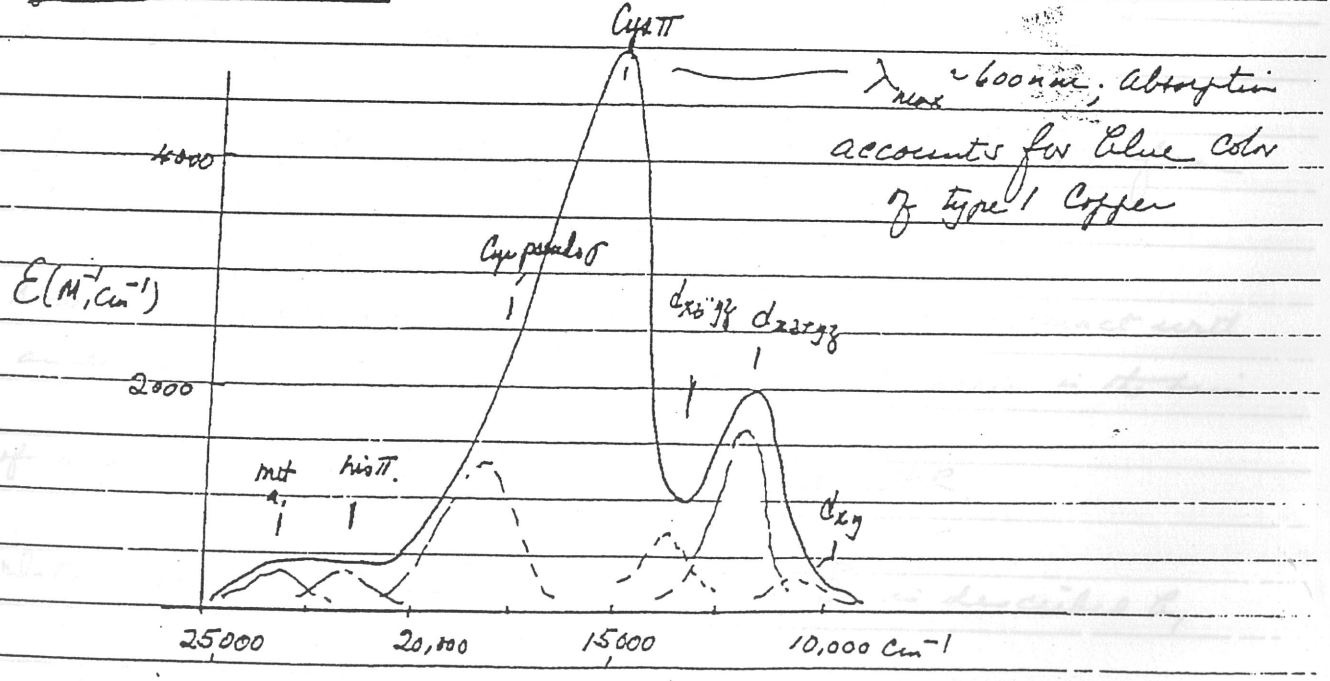

EPR ≡ Electron Paramagnetic Resonance
(also ESR ≡ electron spin resonance)

Another spectroscopic handle to monitor the electronic structure of metal site in metalloprotein is EPR. This is a rather technical subject, so I thought I would give you a short course on the subject.

For a copper II complex or a d^9 copper site in a protein, there are 9 e^- in the d-shell. Q.M., this is equivalent to one electron hole in d-shell.

For an D_{4h} copper complex, we may write

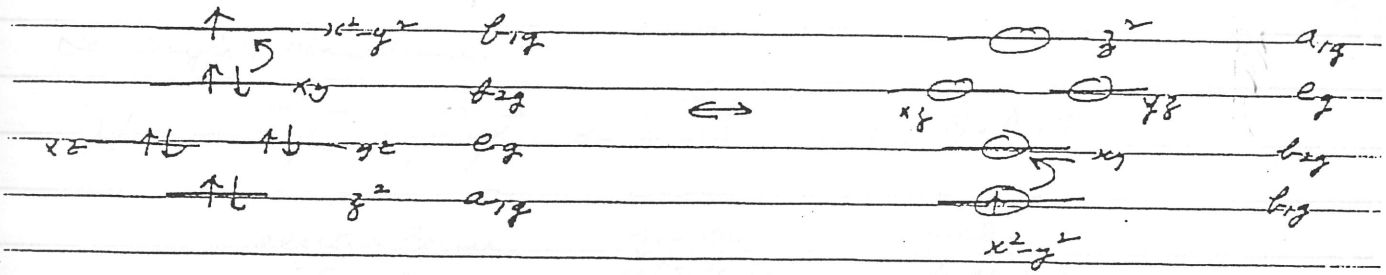

electrons in d-shell
or electrons occupying d-orbitals

electron hole occupying
d-like states

d-d optical transitions correspond to excitations of the hole from 1 hole state to another.

Now unpaired electrons and unpaired electron holes interact with an external magnetic field ($\vec{H}$) and this interaction is the basis ($\vec{B}$)
of a form of spectroscopy (μwave) called EPR.

Interaction of unpaired e^- with $\vec{H}$ or $\vec{B}$ is described by

$$\mathcal{H}_Z = -\vec{\mu}_S \cdot \vec{H} - \vec{\mu}_L \cdot \vec{H} = -\vec{H} \cdot \vec{\mu}_S - \vec{H} \cdot \vec{\mu}_L$$

To complete the description, must include interaction of electron spin or $\vec{\mu}_S$ with the magnetic field produced by orbital motion of the e^-. This interaction is called spin-orbital interaction and is usually written as

$\lambda \vec{L} \cdot \vec{S}$ where $\vec{L}$ = angular momentum associated with e^-

$\vec{S}$ = electron spin

λ is the spin-orbit coupling parameter.

We must also include the possibility of magnetic nuclei in the vicinity of unpaired electron(s) and that these magnetic nuclei interact with the applied magnetic field and with the unpaired electron(s) (as well as with each other)

So complete Hamiltonian

$$\mathcal{H} = \underbrace{-\vec{H}\cdot\vec{\mu}_S - \vec{H}\cdot\vec{\mu}_L}_{\text{electron Zeeman interaction}} + \underbrace{\lambda \vec{L}\cdot\vec{S}}_{\text{spin-orbit interaction}} + \underbrace{\vec{S}\cdot A\cdot\vec{I}}_{\text{nuclear hyperfine interaction}}$$

$$+ \underbrace{\sum_{N'} \vec{S}\cdot A_{N'}\cdot\vec{I}_{N'}}_{\substack{\text{ligand} \\ \text{magnetic} \\ \text{nuclei}}} - \underbrace{\sum_{N} \vec{H}\cdot\vec{\mu}_N}_{\substack{\text{all} \\ \text{nuclei}}}$$

superhyperfine interaction — nuclear Zeeman interaction

where I is the nuclear spin of the transition metal ion

N' refers to magnetic nuclei associated with the ligands

eg. ^1H, ^{14}N, ^{13}C, ^{15}N etc.

introduced

The terms are written in the order of decreasing importance, except that in the case of proton hyperfine, nuclear Zeeman is typically larger than nuclear hyperfine interaction.

Now for unpaired e^- or hole,

electron g-values

$$-\vec{\mu}_S = +g_S \beta \vec{S} = +2.0023\,\beta \vec{S} \qquad g_S = 2.0023$$

$$g_L = 1.0000$$

and $$-\vec{\mu}_L = +g_L \beta \vec{L} = +1.0000\,\beta \vec{L}$$

where β = Bohr magneton $= \dfrac{e\hbar}{2m_e c}$

Since the spectral positions of the main features of an EPR spectrum are determined by the electron Zeeman interaction and spin-orbit interaction, we shall consider these interactions first. Remaining interactions are responsible for the fine-structure in the spectrum.

Electron Zeeman Interaction (to first-order)

$$\mathcal{H}_{\text{electron Zeeman}} = +g_S \beta \vec{H}\cdot\vec{S} + 1.0000\,\beta \vec{H}\cdot\vec{L} + \lambda \vec{L}\cdot\vec{S}$$

$$+\mathcal{H}_{\text{spin-orbit}}$$

Energy to first order $W_{m_S} = g_S \beta H_0 m_S + 0 + 0$

vanishes to first order because $\vec{L}$ is quenched by ligand field, i.e., $\langle \vec{L} \rangle = 0$

It's instructive to examine the first term more closely.

Let's consider our D_{4h} complex

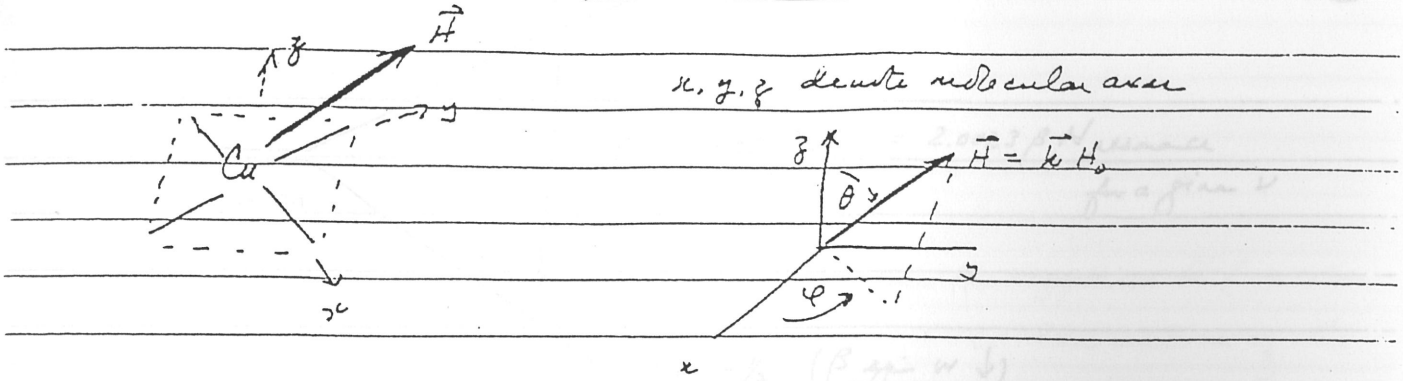

Note that we can write $g_s \beta \vec{H} \cdot \vec{S}$ as

$$g_s \beta \begin{pmatrix} H_x & H_y & H_z \end{pmatrix} \begin{pmatrix} S_x \\ S_y \\ S_z \end{pmatrix}$$

$$= g_s \beta \begin{pmatrix} H_0 \sin\theta \cos\varphi & H_0 \sin\theta \sin\varphi & H_0 \cos\theta \end{pmatrix} \begin{pmatrix} S_H \sin\theta \cos\varphi \\ S_H \sin\theta \sin\varphi \\ S_H \cos\theta \end{pmatrix}$$

$$= g_s \beta H_0 \underbrace{\left(\sin^2\theta \cos^2\varphi + \sin^2\theta \sin^2\varphi + \cos^2\theta \right)}_{1} S_H$$

$$= g_s \beta H_0 S_H$$

In q.m., S_H is quantized along $\vec{H}$ so that $\langle S_H \rangle = m_s = \pm 1/2$

Therefore energy levels of electron spin are given to first order by

$$g \beta H_0 m_s \quad \text{with } m_s = \pm 1/2$$

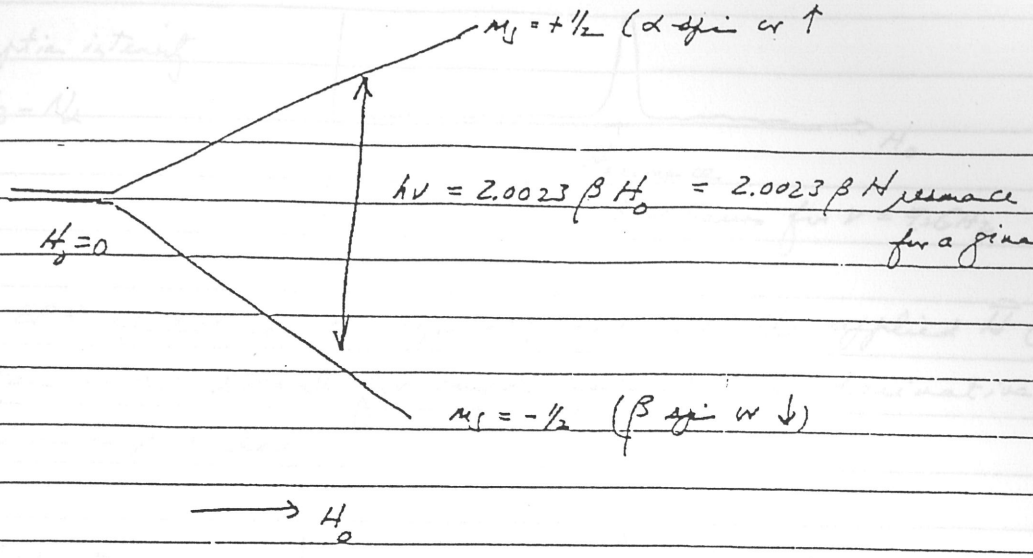

EPR spectra is usually obtained by fixing frequency of observation

$\nu = 9 \times 10^9$ Hz $\quad \frac{\nu}{c} = \frac{9 \times 10^9}{3 \times 10^{10}}\ cm^{-1} = 0.3\ cm^{-1}$

or $\lambda = \frac{c}{\nu} = 3$ cm $\quad$ Microwave

X-Band

$\nu = 35 \times 10^9$ Hz $\quad \frac{\nu}{c} = \frac{35 \times 10^9}{3 \times 10^{10}}\ cm^{-1} \simeq 1\ cm^{-1}$

or $\lambda = 1$ cm $\quad$ Microwave

Q-Band

$\nu = 3 \times 10^9$ Hz $\quad \frac{\nu}{c} = \frac{3 \times 10^9}{3 \times 10^{10}} \simeq 0.1\ cm^{-1}$

or $\lambda = 10$ cm $\quad$ Microwave

S-Band

and varying H_0 to achieve resonance.

X-Band $\quad H_0 = 3400$ Gauss for $\nu = 9.5 \times 10^9$ Hz

3300 Gauss for $\nu = 9.2 \times 10^9$ Hz

Q-Band $\quad$ 12,500 Gauss for $\nu = 35 \times 10^9$ Hz

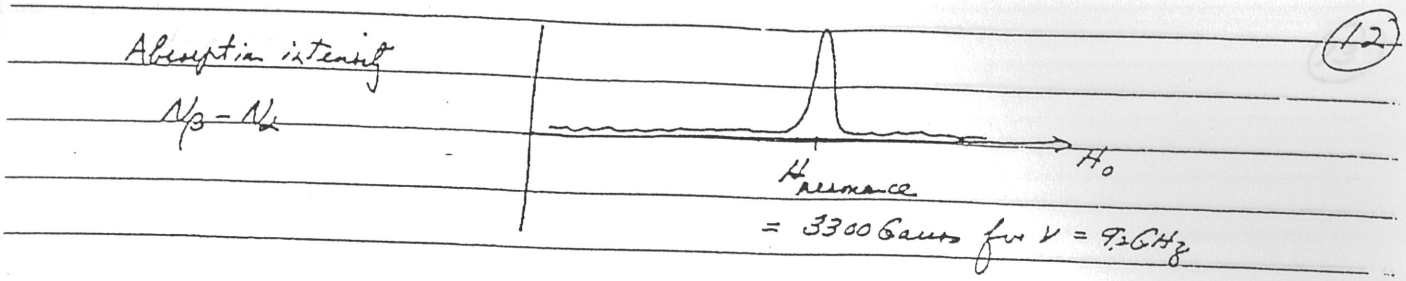

Since in EPR spectroscopy, we typically modulate the applied $\vec{H}$ (in order to obtain an a.c. signal for amplification), the derivative of the absorption is recorded.

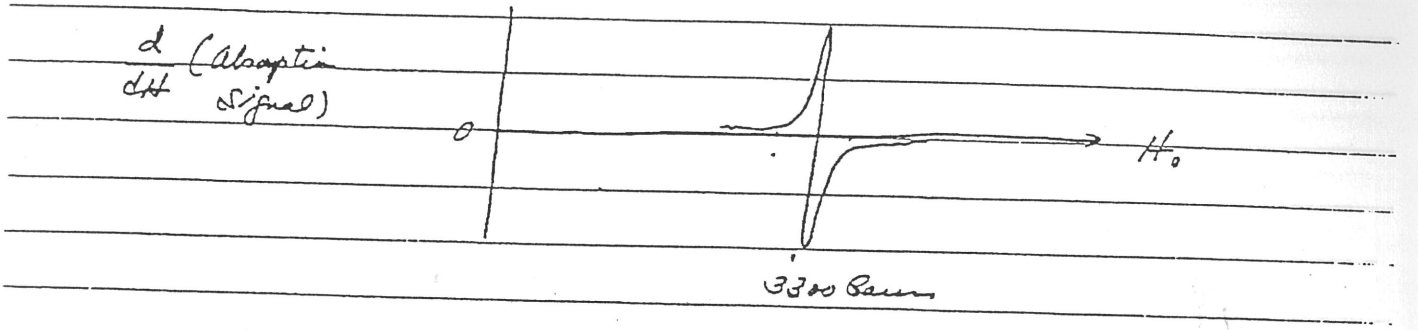

Zeeman Interaction (to second order)

The above treatment of the Zeeman interaction (to first order) assumes that the spin is totally decoupled from the orbital motion of the electron, which, of course, is not true. The spin-orbit interaction couples them. We now correct for this spin-orbit coupling to obtain the Zeeman energy to second order.

Return to model complex

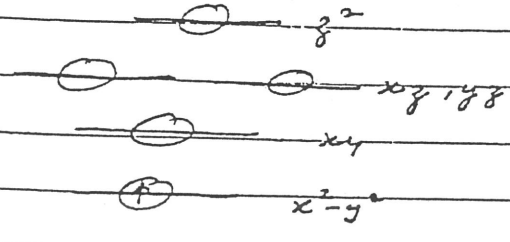

$d_{z^2} = d_0$

$d_{xz}, d_{yz} = \frac{1}{\sqrt{2}}(d_1 \pm d_{-1})$

$d_{xy} = \frac{1}{\sqrt{2}}(d_2 - d_{-2})$

$d_{x^2-y^2} = \frac{1}{\sqrt{2}}(d_2 + d_{-2})$

Wavefunction for hole = $d_{x^2-y^2} \cdot \alpha$ spin ↑

$d_{x^2-y^2} \cdot \beta$ spin ↓

d-orbitals

$$d_2 = \sqrt{\frac{15}{8\pi}} \times f(r) \times \left(\frac{1}{4}\sin^2\theta\, e^{2i\phi}\right)$$

$$d_1 = \text{"} \times \left(-\sin\theta\cos\theta\, e^{i\phi}\right)$$

$$d_0 = \text{"} \times \left(\frac{1}{16}(3\cos^2\theta - 1)\right)$$

$$d_{-1} = \text{"} \times \left(+\sin\theta\cos\theta\, e^{-i\phi}\right)$$

$$d_{-2} = \text{"} \times \left(\frac{1}{4}\sin^2\theta\, e^{-2i\phi}\right)$$

Because of spin-orbit interaction, wave function for hole is no longer $d_{x^2-y^2}\cdot\alpha$ or $d_{x^2-y^2}\cdot\beta$ and must be corrected!

Denote spin up state by ψ_+ & spin-down state by ψ_-

From perturbation theory, one can show that

$$\psi_+ = d_{x^2-y^2}\cdot\alpha - \sum_{\substack{i=xy \\ yz,xz \\ z^2 \\ m_s=\pm\frac{1}{2}}} \frac{\left(\int d_i^* \cdot \phi_{m_s}^* \left(\lambda \vec{L}\cdot\vec{S}\right) d_{x^2-y^2}\cdot\alpha\right) d\tau}{E(d_i\cdot\phi_{m_s}) - E(d_{x^2-y^2}\cdot\alpha)}\, d_i\cdot\phi_{m_s}$$

where d_i refers to i d-orbital

ϕ_{m_s} refer to appropriate spin function

$\left(\phi_{+\frac{1}{2}} \rightarrow \alpha \;;\; \phi_{-\frac{1}{2}} \rightarrow \beta\right)$

and $\psi_- = d_{x^2-y^2}\cdot\beta - \sum_{\substack{i=xy, \\ \forall z,x \\ z^2 \\ m_s=\pm\frac{1}{2}}} \frac{\int d_i^* \cdot \phi_{m_s}^* \;\lambda \vec{L}\cdot\vec{S}\; d_{x^2-y^2}\cdot\beta\; d\tau}{E(d_i\cdot\phi_{m_s}) - E(d_{x^2-y^2}\cdot\beta)}\, d_i\cdot\phi_{m_s}$

Since $\vec{L}\cdot\vec{S} = L_z S_z + L_x S_x + L_y S_y$

$= L_z S_z + \frac{1}{2}(L^+S^- + L^-S^+)$

$\hat{L_z}\hat{S_z}$ mixes in some $d_{xy}\cdot\alpha$ with $d_{x^2-y^2}\cdot\alpha$

and $d_{xy}\cdot\beta$ with $d_{x^2-y^2}\cdot\beta$

$\hat{L^+S^-}$ mixes in some $d_1\cdot\beta$ with $d_{x^2-y^2}\cdot\alpha$

$\hat{L^-S^+}$ mixes in some $d_{+1}\cdot\beta$ with $d_{x^2-y^2}\cdot\alpha$

If do algebra, we find

$$\psi_+ = d_{x^2-y^2}\cdot\alpha - \frac{\lambda}{\Delta_1} d_{xy}\cdot\alpha - \frac{1}{\sqrt{2}}\frac{\lambda}{\Delta_2} d_{-1}\cdot\beta$$

and

$$\psi_- = d_{x^2-y^2}\cdot\beta + \frac{\lambda}{\Delta_1} d_{xy}\cdot\beta - \frac{1}{\sqrt{2}}\frac{\lambda}{\Delta_2} d_{+1}\cdot\alpha$$

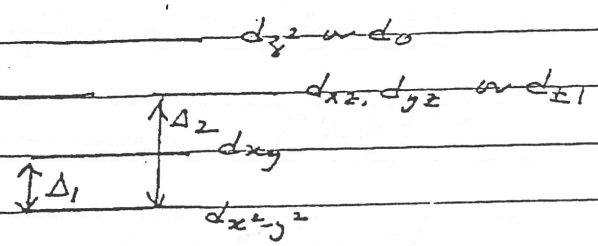

Next to use these corrected wavefunction to obtain Zeeman energy to second order.

Recall Zeeman interaction given by

$$\mathcal{H}_Z = +g_s\beta\vec{H}\cdot\vec{S} + 1.0000\beta\vec{H}\cdot\vec{L}$$

$$= \beta \begin{pmatrix} H_x & H_y & H_z \end{pmatrix} \begin{pmatrix} g_s S_x + L_x \\ g_s S_y + L_y \\ g_s S_z + L_z \end{pmatrix}$$

Let's say magnetic field is along z-direction

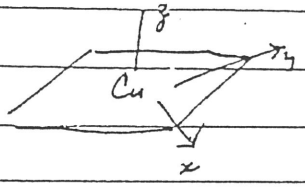

$$\hat{\mathcal{H}}_I = \beta H_z (g_s \hat{S}_z + \hat{L}_z) = \beta H_0 (g_s \hat{S}_z + \hat{L}_z)$$

$$\text{Zeeman energy} = \int \psi_{\pm}^* \beta H_0 (g_s \hat{S}_z + \hat{L}_z) \psi_{\pm} \, d\tau$$

$$= \beta H_0 \left[(g_s)(\pm \tfrac{1}{2}) \mp \frac{4\lambda}{\Delta_1} + \text{higher order terms} \right]$$

$$\cong \beta H_0 (\pm \tfrac{1}{2}) \left[g_s - \frac{8\lambda}{\Delta_1} \right]$$

$$\cong \beta H_0 (\pm \tfrac{1}{2}) g_s \left(1 - \frac{4\lambda}{\Delta_1} \right)$$

Define effective g-value $\equiv g_{11}$ when H is along z axis

$$\text{Zeeman energy} = \beta H_0 (\pm \tfrac{1}{2}) g_{11}$$

$$\therefore g_{11} = g_s \left(1 - \frac{4\lambda}{\Delta_1} \right)$$

For Cu, $\lambda = -829 \text{ cm}^{-1}$

Define $\varphi = -\lambda = +829 \text{ cm}^{-1}$

$$\boxed{g_{11} = g_s \left(1 + \frac{4\varphi}{\Delta_1} \right)} \quad > g_s$$

When magnetic field is in x-y plane, say along x-direction

$$\hat{\mathcal{H}}_z = \beta H_0 (g_s \hat{S}_x + \hat{L}_x)$$

$$\text{Zeeman energy} = \int \psi_\pm^* \beta H_0 (g_s \hat{S}_x + \hat{L}_x) \psi_\pm \, d\tau$$

$$= 0$$

But $$\int \psi_\pm^* \beta H_0 [g_s \hat{S}_x + \hat{L}_x] \psi_\mp \, d\tau \neq 0$$

So correct $\psi_x^\pm = \frac{1}{\sqrt{2}} (\psi_+ \pm \psi_-)$

$$\underset{\sim}{\mathcal{H}_z} = \begin{matrix} \\ \psi_+ \\ \psi_- \end{matrix} \begin{matrix} \begin{matrix} \psi_+ & \psi_- \end{matrix} \\ \begin{pmatrix} 0 & -\frac{\lambda}{\Delta_2} + g_s\left(\frac{1}{2}\right) \\ -\frac{\lambda}{\Delta_2} + g_s\left(\frac{1}{2}\right) & 0 \end{pmatrix} \end{matrix} \beta H_0$$

● Zeeman energies (obtained by diagonalizing 2×2)

$$= \pm \beta H_0 \left(g_s \tfrac{1}{2} - \frac{\lambda}{\Delta_2} \right)$$

$$\cong \pm \beta H_0 \tfrac{1}{2} g_s \left(1 - \frac{\lambda}{\Delta_2}\right)$$

Define effective g-value $\equiv g_x$ when H is along x-axis

$$\text{Zeeman energy} = \beta H_0 \left(\pm \tfrac{1}{2}\right) g_x$$

$$\therefore g_x = g_s \left(1 - \frac{\lambda}{\Delta_2}\right) = g_s \left(1 + \frac{2}{\Delta_2}\right)$$

Identical result obtained for g_y, $\therefore$ define $g_\perp = g_x = g_y$

$$g_\perp = g_x = g_y = g_s \left(1 - \frac{\lambda}{\Delta_2}\right) = g_s \left(1 + \frac{2}{\Delta_2}\right) > g_s$$

But $\Delta_2 \gg \Delta_1$ $\therefore$ $g_{\parallel} > g_\perp > g_s$

Arbitrary orientations of H_0 $\vec{H}$ w.r.t. x, y, z

$\beta \vec{H} \cdot \underset{\sim}{g} \cdot \vec{S}$ where $\underset{\sim}{g} \equiv$ g-tensor

$$= \beta \begin{pmatrix} H_x & H_y & H_z \end{pmatrix} \begin{pmatrix} g_\perp & 0 & 0 \\ 0 & g_\perp & 0 \\ 0 & 0 & g_\parallel \end{pmatrix} \begin{pmatrix} S_x \\ S_y \\ S_z \end{pmatrix}$$

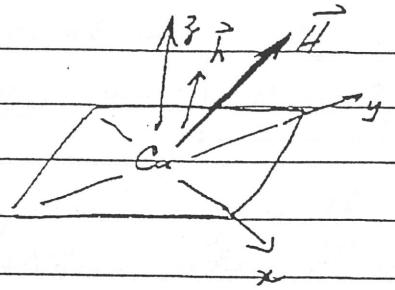

$\vec{h}$ — direction of effective field

$\vec{S}_H$

Because of g anisotropy, $\vec{S}$ is no longer quantized along $\vec{H}$, but along a direction given by $\vec{H} \cdot \underset{\sim}{g}$

Let's denote the direction of $\vec{H} \cdot \underset{\sim}{g}$ by unit vector $\vec{h}$ and its magnitude by $H_0 g_{eff}$

Then $\vec{h} H_0 g_{eff} = \vec{H} \cdot \underset{\sim}{g}$

Since $H_0^2 g_{eff}^2 = (\vec{H} \cdot \underset{\sim}{g})(\underset{\sim}{g} \cdot \vec{H}) = \vec{H} \cdot \underset{\sim}{g^2} \cdot \vec{H}$

$$= H_0^2 (\sin\theta\cos\varphi \;\; \sin\theta\sin\varphi \;\; \cos\theta) \cdot \underset{\sim}{g^2} \cdot \begin{pmatrix} \sin\theta\cos\varphi \\ \sin\theta\sin\varphi \\ \cos\theta \end{pmatrix}$$

$$\underset{\sim}{g^2} = \begin{pmatrix} g_\perp & 0 & 0 \\ 0 & g_\perp & 0 \\ 0 & 0 & g_\parallel \end{pmatrix} \begin{pmatrix} g_\perp & 0 & 0 \\ 0 & g_\perp & 0 \\ 0 & 0 & g_\parallel \end{pmatrix} = \begin{pmatrix} g_\perp^2 & 0 & 0 \\ 0 & g_\perp^2 & 0 \\ 0 & 0 & g_\parallel^2 \end{pmatrix}$$

$$= H_0^2 (\sin\theta\cos\varphi \;\; \sin\theta\sin\varphi \;\; \cos\theta) \begin{pmatrix} g_\perp^2 & 0 & 0 \\ 0 & g_\perp^2 & 0 \\ 0 & 0 & g_\parallel^2 \end{pmatrix} \begin{pmatrix} \sin\theta\cos\varphi \\ \sin\theta\sin\varphi \\ \cos\theta \end{pmatrix}$$

$$= H_0^2 \left[(\sin^2\theta\cos^2\varphi) g_\perp^2 + \sin^2\theta\sin^2\varphi) g_\perp^2 + \cos^2\theta \, g_\parallel^2 \right]$$

or $g_{eff} = \left(g_\perp^2 \sin^2\theta \cos^2\varphi + g_\perp'^2 \sin^2\theta \sin^2\varphi + g_\parallel^2 \cos^2\theta\right)^{1/2}$

and the EPR transition occurs at

$$\boxed{h\nu = \left(g_\perp^2 \sin^2\theta \cos^2\varphi + g_\perp'^2 \sin^2\theta \sin^2\varphi + g_\parallel^2 \cos^2\theta\right)^{1/2} \beta H_0}$$

So for a given ν, $H_{resonance}$ will depend on θ, φ.

For the axial case, $H_{resonance}$ depends on θ only, since $g_\perp = g_\perp'$ and $\boxed{h\nu = \left(g_\perp^2 \sin^2\theta + g_\parallel^2 \cos^2\theta\right)^{1/2} \beta H_0}$

These expressions give the resonance fields in single crystal studies, when $\vec{H}$ is oriented at defined orientations wrt to x, y, z (molecular axes), or principal axes of g tensor

Powder Spectrum

all orientations of x, y, z with respect to $\vec{H}$ are present in a powder sample. So EPR spectrum observed is a superposition of absorptions from all possible orientations $\Rightarrow$ called a powder spectrum. For an axial Cu complex, where $g_\parallel > g_\perp$

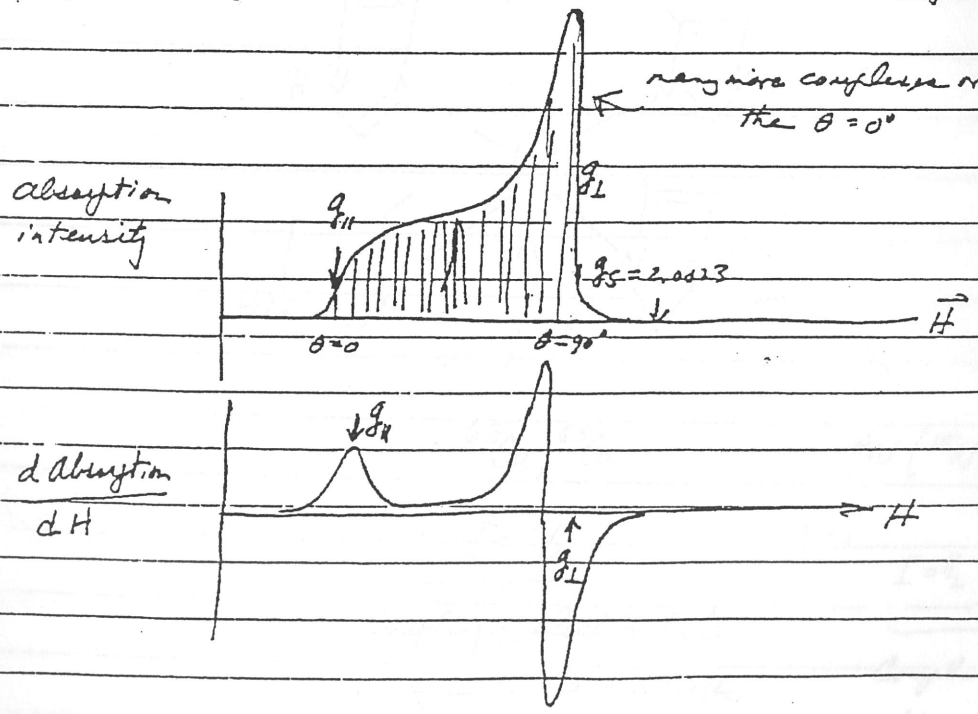

Lecture 3 February 9, 1993

Nuclear hyperfine interaction in EPR spectroscopy of transition metal complexes

Interaction of unpaired e^- (or hole) with nuclear spin of transition metal ion and magnetic nuclei of ligands

$$\vec{S} \cdot \underset{\sim}{A} \cdot \vec{I} + \sum_{N'} \vec{S} \cdot A_{N'} \cdot \vec{I}_{N'} - \sum_{N} \vec{H} \cdot \mu_N$$

N': magnetic nuclei on ligands

N: all magnetic nuclei

- $\vec{S} \cdot \underset{\sim}{A} \cdot \vec{I}$: nuclear hyperfine interaction
- $\sum_{N'} \vec{S} \cdot A_{N'} \cdot \vec{I}_{N'}$: nuclear superhyperfine interaction
- $\sum_{N} \vec{H} \cdot \mu_N$: nuclear Zeeman interaction

Example

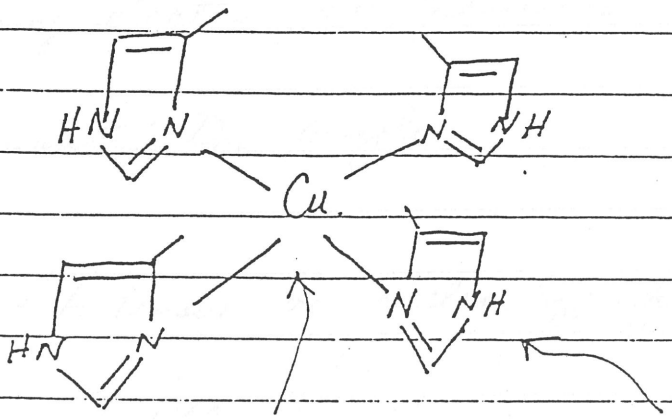

$Cu(Im)_4^{++}$

^{63}Cu, ^{65}Cu — $I = 3/2$

Coupling of electron hole or spin to Cu nucleus → nuclear hyperfine interaction

^{14}N (^{15}N): $I = 1$; ^{1}H: $I = 1/2$; ^{13}C: $I = 1/2$

Coupling of electron hole or spin to ligand magnetic nuclei → superhyperfine interaction

Focus on nuclear hyperfine interaction

$$\vec{S} \cdot A \cdot \vec{I} - \vec{\mu}_N \cdot \vec{H}$$

Since $\vec{\mu}_N = g_I \beta_N \vec{I}$, where $g_I \equiv$ nuclear g-value

β_N = nuclear Bohr magneton

$$= \frac{e\hbar}{2M_p c}$$

Can rewrite as

$$\vec{S} \cdot A \cdot \vec{I} - g_I \beta_N \vec{H} \cdot \vec{I} = -g_I \beta_N (\vec{H}_e + \vec{H}) \cdot \vec{I}$$

where $g_I \beta_N \vec{H}_e = -\vec{S} \cdot \underset{\sim}{A}$

or $$g_I \beta_N (H_{ex} \; H_{ey} \; H_{ez}) = -(S_x \; S_y \; S_z) \begin{pmatrix} A_{xx} & A_{xy} & A_{xz} \\ A_{yx} & A_{yy} & A_{yz} \\ A_{zx} & A_{zy} & A_{zz} \end{pmatrix}$$

Can refer $\vec{H}_e$ as the magnetic field produced by spinning electron at transition metal nucleus.

Pick symmetric D_{4h} complex

$\underset{\sim}{A}$ = "A" tensor or nuclear hyperfine tensor

$$= \begin{pmatrix} A_{xx} & 0 & 0 \\ 0 & A_{yy} & 0 \\ 0 & 0 & A_{zz} \end{pmatrix} = \begin{pmatrix} A_\perp & 0 & 0 \\ 0 & A_{\perp'} & 0 \\ 0 & 0 & A_\parallel \end{pmatrix}$$

Then $$g_I \beta_N (H_{ex} \; H_{ey} \; H_{ez}) = -(S_x A_\perp \;\; S_y A_{\perp'} \;\; S_z A_\parallel)$$

So total magnetic field experienced by magnetic nucleus

is given by $\left(H_x - \frac{A_\perp S_x}{g_I \beta_N}, H_y - \frac{A_\perp' S_y}{g_I \beta_N}, H_z - \frac{A_\parallel S_z}{g_I \beta_N}\right)$

and the effective Hamiltonian for the problem becomes

$$\beta (H_x\ H_y\ H_z) \begin{pmatrix} g_\perp & 0 & 0 \\ 0 & g_\perp' & 0 \\ 0 & 0 & g_\parallel \end{pmatrix} \begin{pmatrix} S_x \\ S_y \\ S_z \end{pmatrix}$$

$$+ \left(A_\perp S_x - g_I \beta_N H_x,\ A_\perp' S_y - g_I \beta_N H_y,\ A_\parallel S_z - g_I \beta_N H_z\right) \begin{pmatrix} I_x \\ I_y \\ I_z \end{pmatrix}$$

(1) For applied magnetic field along z-axis

$$H_x = 0,\ H_y = 0,\ H_z = H_0$$

$$\text{Hamiltonian} = \beta H_0 g_\parallel S_z + A_\perp S_x I_x + A_\perp' S_y I_y + A_\parallel S_z I_z$$

$$- g_I \beta_N H_0 I_z$$

$\vec{S}$ and $\vec{I}$ are both quantized along $\vec{H}$

$\therefore \langle S_z \rangle = \pm \frac{1}{2}$ $\qquad \langle I_z \rangle = m_I$

$\langle S_x \rangle = 0$ $\qquad \langle I_x \rangle = 0$

$\langle S_y \rangle = 0$ $\qquad \langle I_y \rangle = 0$

$$\text{Energy} = \beta H_0 g_\parallel m_S + A_\parallel m_S m_I - g_I \beta_N H_0 m_I$$

EPR Selection rule $\Delta m_S = \pm 1$, $\Delta m_I = 0$

$$h\nu = \beta H_0 g_{\parallel} + A_{\parallel} m_I$$

(2) For applied magnetic field along x-axis

$$H_x = H_0, \quad H_y = 0, \quad H_z = 0$$

$$\text{Hamiltonian} = \beta H_0 g_{\perp} S_x + A_{\perp} S_x I_x + A_{\perp} S_y I_y + A_{\parallel} S_z I_z - g_I \beta_N H_0 I_x$$

$$\text{Energy} = \beta H_0 g_{\perp} m_S + A_{\perp} m_S m_I - g_I \beta_N H_0 m_I$$

and EPR transition occur at

$$h\nu = \beta H_0 g_{\perp} + A_{\perp} m_I$$

Return to Cu(II) complexes

2 Cu isotopes :	^{63}Cu	69.09%	$I = 3/2$	7.1088
	^{65}Cu	30.91%	$I = 3/2$	7.6104

Therefore observed powder spectrum is a superposition of eight powder (sub-) spectra, one for each of the m_I's for the two Cu isotopes. But g_I's for the two Cu isotopes differ by <10%. So for all practical purposes, can interpret the observed spectrum as a superposition of four "powder (sub-) spectra"

Expected spectrum sum of following 4 subspectra:

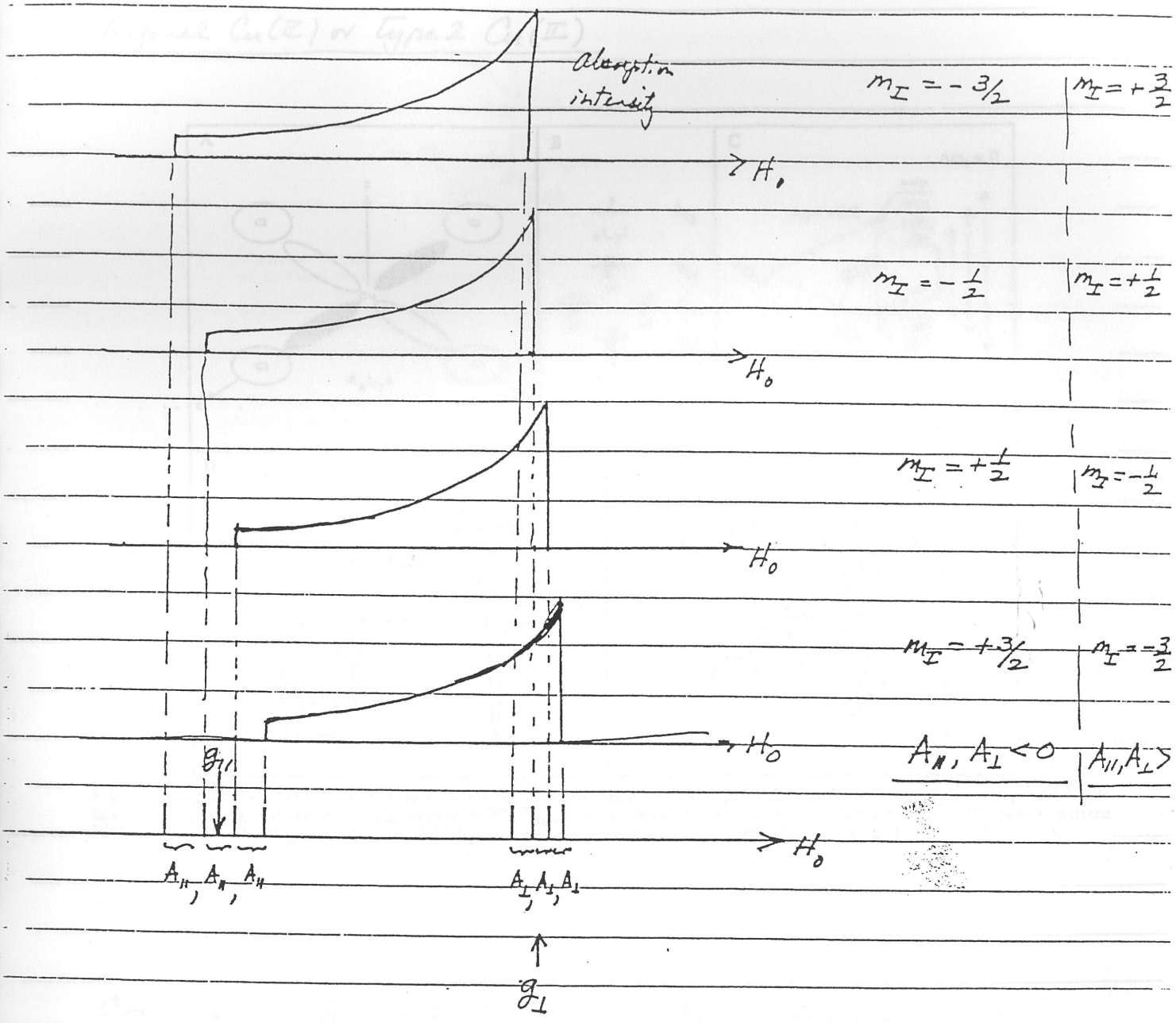

I have assumed that A_{II} and $A_\perp$ are of the same sign, but that need not be the case.

Composite spectrum

not to scale

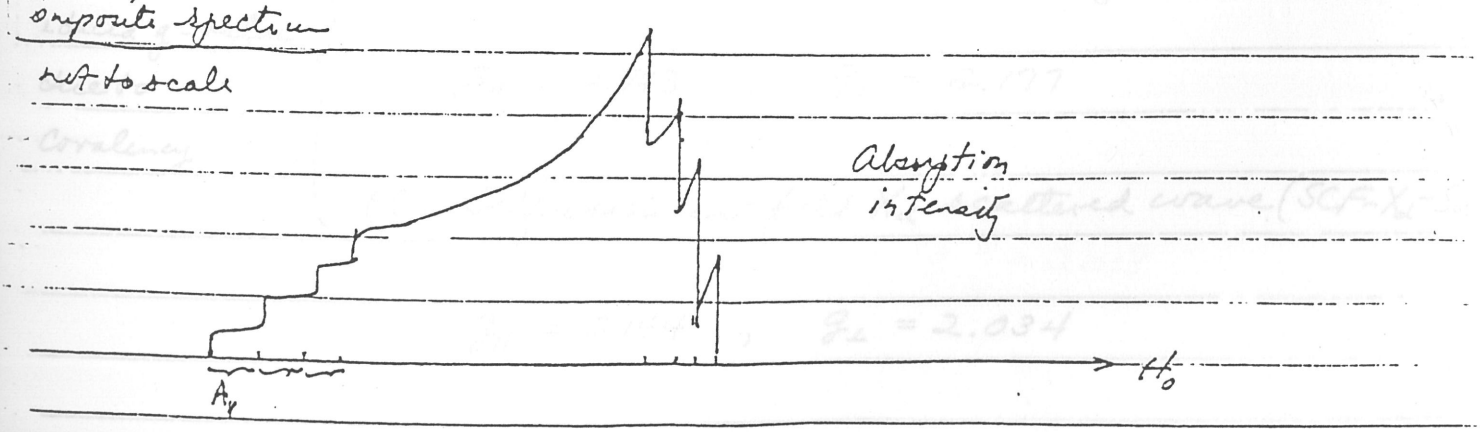

Experiments (Data taken from Solomon's review in Chem. Reviews)

Tetragonal Cu(II) or type 2 Cu(II)

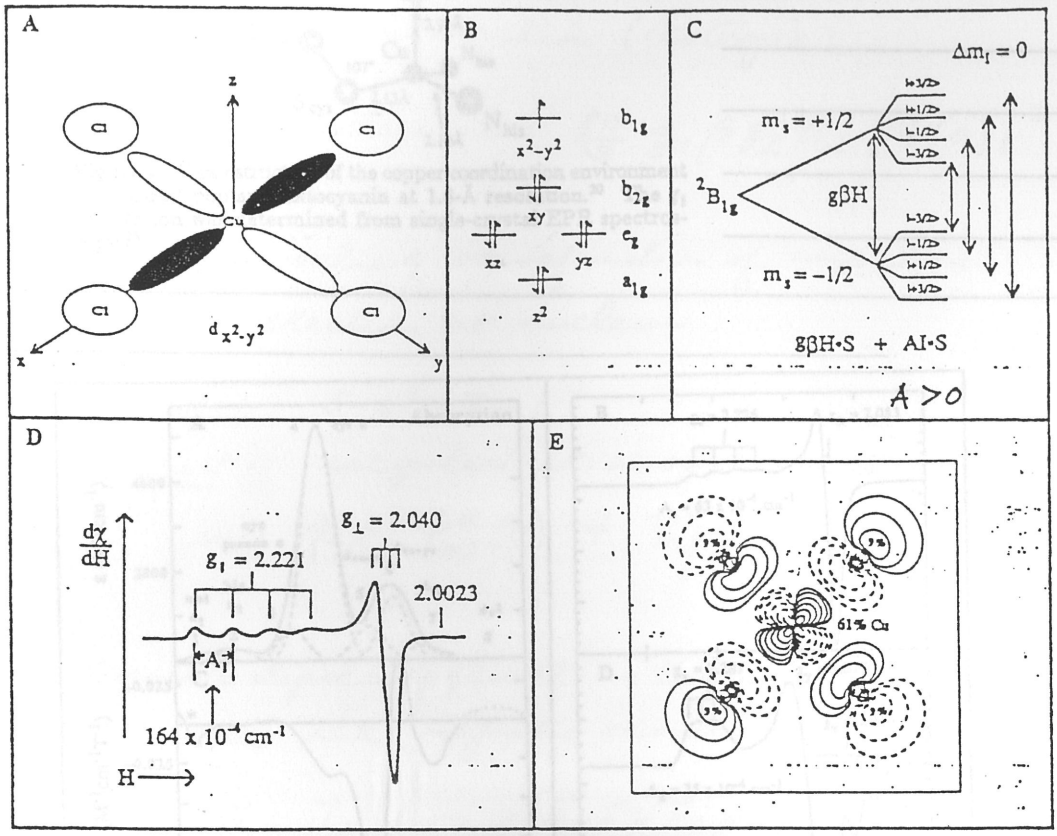

Figure 1. Ligand-field theory and ground-state electronic properties of normal cupric complexes: (A) square planar D_{4h}-$CuCl_4^{2-}$; (B) ligand field splitting of d orbitals in D_{4h} symmetry; (C) $^2B_{1g}$ ground-state Zeeman and hyperfine splitting diagram; (D) powder pattern EPR spectrum of the $^2B_{1g}$ ground state; (E) $^2B_{1g}$ ground-state wave function from adjusted-sphere SCF-Xα-SW calculation.

Observed $g_{11} = 2.221$, $g_\perp = 2.040$

Predicted (a) ligand-field (no covalent delocalization of metal d-orbitals onto ligand valence orbitals)

reduced g-values due to covalency

$g_{11} = 2.743$, $g_\perp = 2.177$

(b) Self-consistent field X_α scattered wave (SCF-X_α-SW)

$g_{11} = 2.144$, $g_\perp = 2.034$

Blue copper site

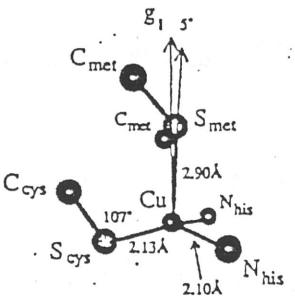

Figure 4. X-ray structure of the copper coordination environment of oxidized poplar plastocyanin at 1.6-Å resolution.[20] The g_1 orientation was determined from single-crystal EPR spectroscopy.[25]

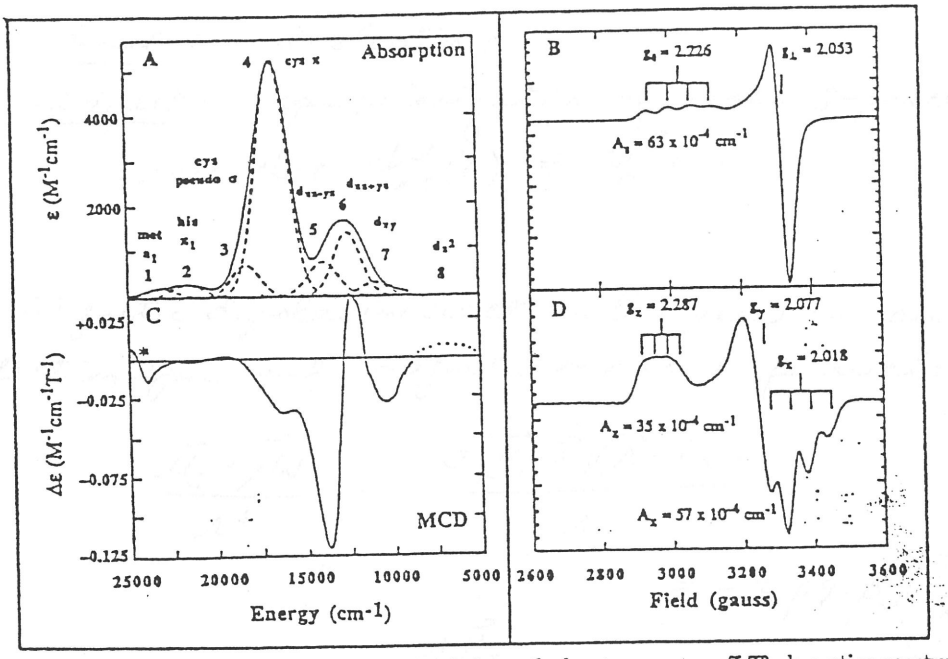

Figure 3. Unique spectral features of blue copper proteins: Part A shows the low-temperature (LT) absorption spectrum of plastocyanin. The dashed lines indicate Gaussian band deconvolution of the spectrum. Assignments of bands 1–8 were determined from LT-absorption and LT-MCD spectroscopies. Part B shows the EPR spectrum of spinach plastocyanin, and C, the LTMCD spectrum of spinach plastocyanin. The dotted portion of the spectrum is estimated from the NIR-LT-MCD spectrum of azurin (see ref 26). The feature marked with an asterisk (*) is due to a small amount of heme impurity. Part D shows the EPR spectrum of stellacyanin.

Observed (for blue copper site in plastocyanin)

$g_{\parallel} = 2.226$, $g_{\perp} = 2.053$

(for blue copper site in stellacyanin)

$g_z = 2.287$; $g_y = 2.077$; $g_x = 2.018$

rhombic!

Understanding $\underline{\underline{A}}$. The nuclear hyperfine interaction

There are 2 contributions to $\underline{\underline{A}}$

(a) Fermi-contact interaction (isotropic)

$$a\,\vec{I}\cdot\vec{S} \quad \text{where } a = \frac{8\pi}{3} g_s \beta g_I \beta_N |\psi(0)|^2$$

where $\psi(0)$ ≡ value of wavefunction of unpaired electron at nucleus

direct : S-electrons

indirect : spin polarization of inner S-shell such that $\psi^{\alpha}_{ns}(0) \neq \psi^{\beta}_{ns}(0)$

(b) Magnetic dipolar interaction between unpaired electron spin and magnetic moment of nucleus

$$\frac{\vec{\mu}_S \cdot \vec{\mu}_N}{r^3} - \frac{3(\vec{\mu}_S\cdot\vec{r})(\vec{r}\cdot\vec{\mu}_N)}{r^5}$$

$$= -g_s \beta g_I \beta_N \left(\frac{\vec{I}\cdot\vec{S}}{r^3} - \frac{3(\vec{I}\cdot\vec{r})(\vec{r}\cdot\vec{S})}{r^5} \right)$$

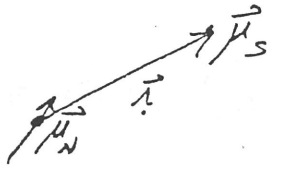

if expand dot-products using cartesian coordinates x, y, z

$$= -g_s \beta g_I \beta_N \left\{ S_x I_x \left\langle \frac{r^2-3x^2}{r^5} \right\rangle + S_y I_y \left\langle \frac{r^2-3y^2}{r^5} \right\rangle + S_z I_z \left\langle \frac{r^2-3z^2}{r^5} \right\rangle \right.$$

where $\langle\ \rangle$ denote averaging over the wavefunction describing the electron spin

$$= T_{xx} S_x I_x + T_{yy} S_y I_y + T_{zz} S_z I_z$$

For Cu(II) complex, with unpaired e^- in "$d_{x^2-y^2}$" orbital

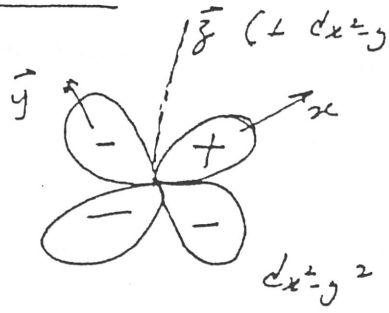

Simple to show that, in this case,

$$T_{xx} = T_{yy} = -\frac{1}{2} T_{zz}$$

and $T_{zz} < 0$ $\quad\because \int (d_{x^2-y^2}) \left(\frac{r^2 - 3z^2}{r^5}\right) d_{x^2-y^2}\, d\tau$

> 0

a turns out to be negative as well because unpaired e^- is in $d_{x^2-y^2}$ orbital, which has a node at Cu nucleus. Only way for $a \neq 0$ is to have spin polarization of inner s-shells by $d_{x^2-y^2}$ electron.

Thus $\quad A_{\parallel} = a + T_{zz} < 0$

$$A_{\perp} = a + T_{xx} = a - \frac{1}{2} T_{zz} \sim 0$$

$< 0 \quad > 0$

$CuCl_4^{2-}$: $\quad |A_{\parallel}| = 164 \times 10^{-4}\ cm^{-1}$

$= 164 \times 10^{-4} \times 3 \times 10^{10}\ Hz$

$= 492\ MHz$

$= \frac{492}{2.8}\ Gauss = 175\ Gauss$ ($A_{\parallel}$ should be < 0)

$|A_{\perp}|$ small

Blue copper site

Plastocyanin : $|A_{//}| = 63 \times 10^{-4}\ cm^{-1} \cong 67$ Gauss

$|A_{\perp}| \sim 0$

Stellacyanin : $|A_{zz}| = 35 \times 10^{-4}\ cm^{-1} = 37$ Gauss

$|A_{xx}| = 57 \times 10^{-4}\ cm^{-1} = 60$ Gauss

Type 3 Copper Centers

Binuclear copper sites

Binuclear copper proteins	MW per Cu_2 site	Function
molluscan hemocyanin	50 kDa	O_2 transport (catalase activity: $2H_2O_2 \longrightarrow 2H_2O + O_2$)
arthropodan hemocyanin	75 kDa	O_2 transport (no catalase activity)
tyrosinase (*neurospora crassa*)	42 kDa	$O_2 + 2H^+ +$ monophenol $\rightarrow$ o-diphenol $+ H_2O$; $O_2 +$ 2 o-diphenol $\rightarrow$ 2 o-quinone $+ 2H_2O$ (catalase activity)

a type 3 copper center is also found in several multicopper oxidases : laccase, ascorbate oxidase (will discuss later).

Hemocyanin

Deoxy Hemocyanin

reactive form

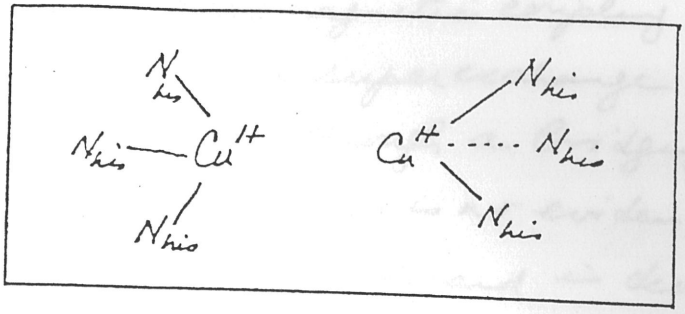

(a) no bridging ligand!
(based on crystal structure at 3.2 Å)
A. Volbeda and W.G. Hol
J. Mol. Biol. (1989) 209, 249-279.

$\downarrow O_2$

(b) $Cu^{1+} \cdots Cu^{1+}$
3.8 Å°

Oxy Hemocyanin

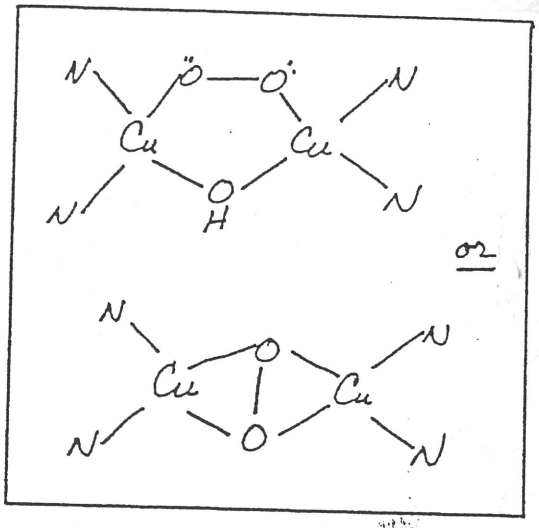

(a) $2Cu^{2+}$ (cupric) based on X-ray spectroscopy

(b) No Cu^{2+} EPR

(c) Magnetic susceptibility indicates strong antiferromagnetic coupling between the two Cu(II) ions to form $S_{Total} = 0$ ground state with the tuplet ($S = 1$ too) higher in energy than the singlet by $> 600\ cm^{-1}$.

(d) EXAFS indicates that two Cu(II) are 3.6 Å apart, too long for direct overlap between the orbitals of the two Cu(II) to give the large

exchange interaction. So antiferromagnetic coupling must involve a superexchange pathway through a bridging ligand. There is no evidence of a bridging ligand in deoxy hemocyanin, so the superexchange pathway must be formed upon dioxygen binding and oxidation of the binuclear copper site.

Oxyhemocyanin

(continue)

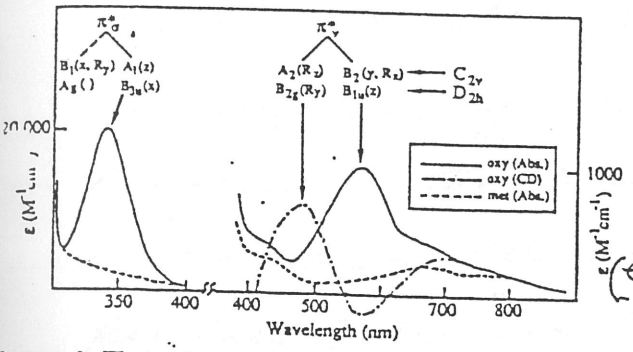

gure 9. Electronic spectra of oxyhemocyanin: absorption and spectra of oxyhemocyanin and absorption spectrum of met hemocyanin, with assignments and selection rules for peroxide-to-copper charge transfer transitions (indicated by arrows) in the and D_{2h} dimer geometries.

(e) Interesting electronic spectrum.

Absorption:

λ_{max} ~ 580 nm (ϵ ~ 1000 $M^{-1}cm^{-1}$)

λ_{max} ~ 350 nm (ϵ ~ 20,000 $M^{-1}cm^{-1}$)

CD

λ_{max} ~ 480 nm (positive)

Oxyhemocyanin

↓ Displacement of Peroxide

Met hemocyanin

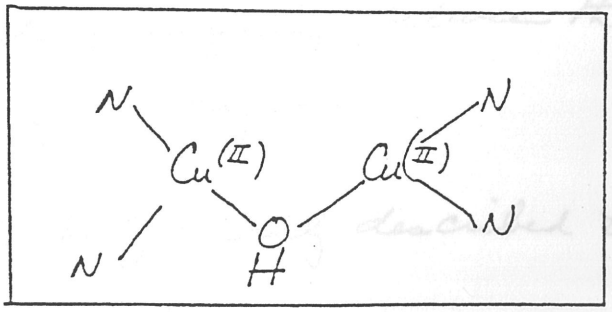

(a) binuclear cupric site

(b) Cu(II)'s strongly antiferromagnetic coupled (based on χ) ⇒ bridging hydroxide

(c) No EPR

(d) Weak d-d bands at 700 nm only.

Structure and electronic structure of oxyhemocyanin

Much of what we presently know about the coordination chemistry (structure and bonding) of hemocyanin binuclear copper site pertains to the oxy form, since this appears to be the form that is most accessible spectroscopically (cf. interesting electronic spectrum). The oxy form is also the most interesting, because it is the oxy form of the binuclear copper cluster in tyrosinase that is important in the catalytic chemistry here, and we would like to delineate those structural/electronic features of the binuclear copper cluster that determine when the site behaves as a monooxygenase (as in tyrosinase) and when it behaves essentially as a reversible dioxygen carrier (as in the hemocyanins)

There have been 3 proposals for the structure of the binuclear copper site in oxy hemocyanin. I shall discuss each of these proposals in turn. Before doing so, let me first discuss the exchange coupling between the two Cu(II) ions in this form of the enzyme.

The exchange interaction is typically described by the spin Hamiltonian

$$\hat{H}_{exchange} = -2J\vec{S}_1 \cdot \vec{S}_2$$

Define $\vec{S}_{Total} = \vec{S}_1 + \vec{S}_2$

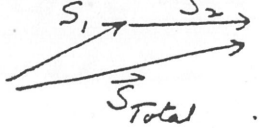

Since $(\vec{S}_1 + \vec{S}_2)\cdot(\vec{S}_1 + \vec{S}_2) = S^2_{Total}$

$$2\vec{S}_1\cdot\vec{S}_2 = \hat{S}^2_{Total} - \hat{S}_1^2 - \hat{S}_2^2$$

$$\langle 2\vec{S}_1\cdot\vec{S}_2\rangle = \left[S_{Total}(S_{Total}+1) - S_1(S_1+1) - S_2(S_2+1)\right]$$

and $W_{exchange} = -2J\langle \vec{S}_1\cdot\vec{S}_2\rangle$

$$= -J\left[S_{Total}(S_{Total}+1) - S_1(S_1+1) - S_2(S_2+1)\right]$$

For 2 d^9 Cu ions, $S_1 = 1/2$, $S_2 = \frac{1}{2}$

$S_{Total} = 0$ or 1

$\therefore W_{exchange} = -J\left[S_{Total}(S_{Total}+1) - \frac{3}{2}\right]$

$W_{exchange}$ (Singlet) $= \frac{3}{2}J$ $\uparrow\downarrow$

$W_{exchange}$ (triplet) $= -\frac{J}{2}$ $\uparrow\uparrow$

<u>Antiferromagnetic coupling</u> $\uparrow\downarrow$ ground state ($S_{Total}=0$)

$J<0$

<u>Ferromagnetic coupling</u> $\uparrow\uparrow$ ground state ($S_{Total}=1$)

$J>0$

For <u>oxy</u> hemocyanin,

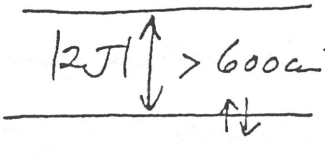

J negative, and $|2J| > 600\,cm^{-1}$.

Proposed structures (or bonding schemes) for oxyhemocyanin binuclear copper site

(I)

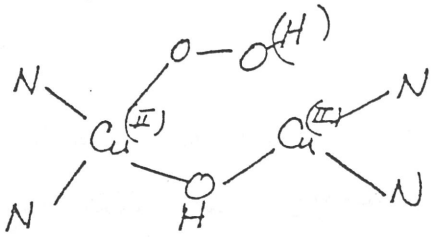

Non-bridging end on hydroperoxide or peroxide

(a) requires hydroxide bridge to mediate superexchange between two cupric ions.

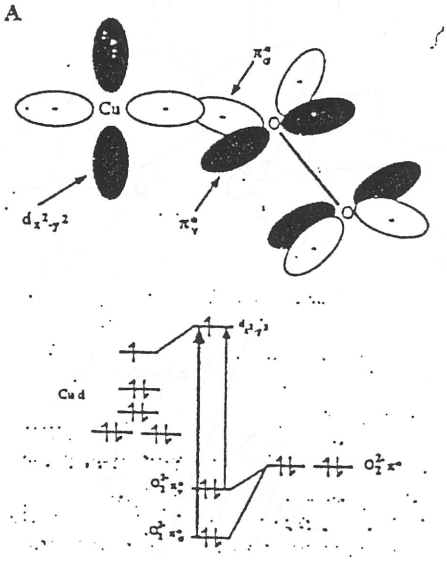

(b) The highest occupied valence orbitals of peroxide are the π^*-degenerate set.

(c) This splits into a π^*_σ and π^*_v upon interaction of peroxide with Cu $d_{x^2-y^2}$ orbital.

The π^*_σ is oriented along the Cu–O bond and has significant σ overlap with the Cu(II) $d_{x^2-y^2}$ orbital.

(d) Excitation of an electron from filled π^*_σ (MO) to half-filled $d_{x^2-y^2}$ Cu orbital (MO) gives rise to a high energy intense O_2^{2-} $\pi^*_\sigma \longrightarrow$ Cu $d_{x^2-y^2}$ charge transfer transition.

(e) π^*_v is oriented perpendicular to Cu–O bond and π-bonding to Cu. Excitation of an electron from filled π^*_v (MO) to half-filled Cu $d_{x^2-y^2}$ orbital (MO)

is expected to lead to a $O_2^{2-}\ \pi^*_\sigma \rightarrow Cu(II)\ d_{x^2-y^2}$ charge transfer transition at lower energy and with much lower intensity than the π^*_σ - charge transfer transition.

These predictions are not in accordance with the observed electronic spectrum of oxyhemocyanin! Thus, it is unlikely that the peroxide is bound to only one Cupric ion end on.

There is, however, a model oxyhemocyanin binuclear Copper cluster that exhibits these spectral features.

Kenneth Karlin Cruse
Kenneth D. Karlin, R.W. Cruse, Y. Haye
Gultneh, A. Farooq, J.C. Hayes
and J. Zubieta
Zubieta Farooq
Gultneh JACS 109, 2668-2679 (1987)

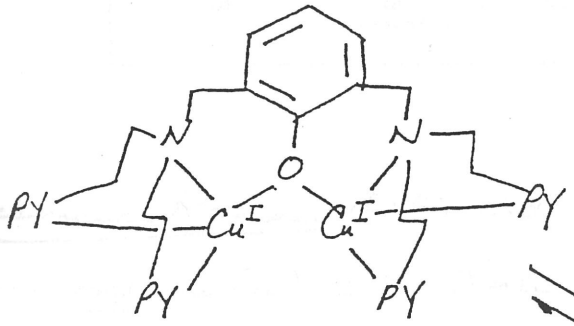

O_2
$-80°C,\ CH_2Cl_2$
$Cu : O_2 = 2:1$

(Orange)

1

CO
PPh_3

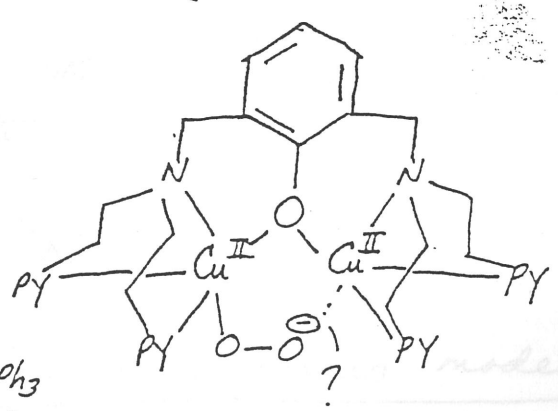

Cu···Cu
3.619 A°

O_2

$L = PPh_3$
CO

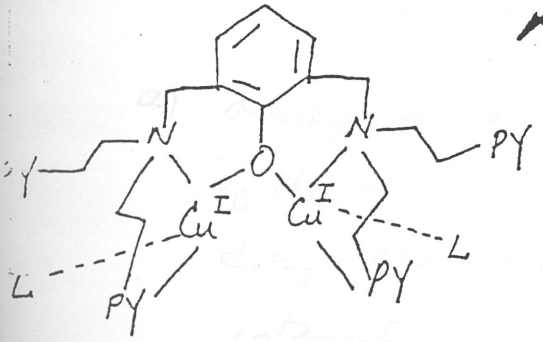

$L = CO$
PPh_3

3

2 dioxygen adduct

(intense purple color)

λ_{max}

505 nm ($\epsilon = 6000\ cm^{-1}M^{-1}$)
610 (shoulder, $\epsilon = 2100$)

385 ($\epsilon = 2900$)
790 ($\epsilon = 700$)
925 ($\epsilon = 600$)

Ligand

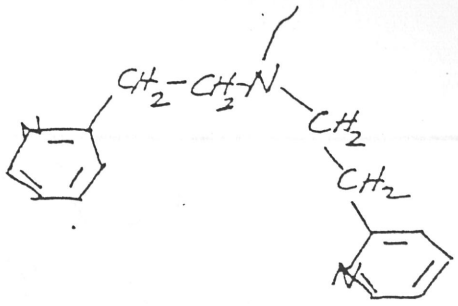

Absorption spectrum

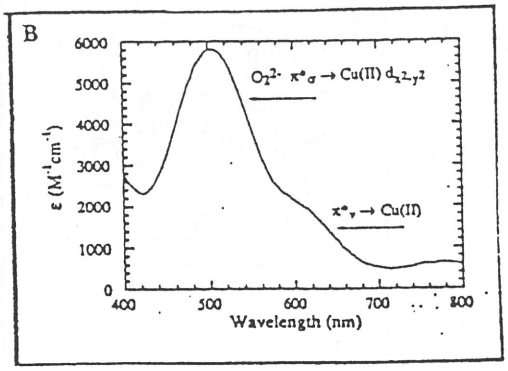

Charge transfer absorption spectrum of peroxide bound to a single Cu (II)

Resonance Raman data indicate that peroxide is bound to only one Cu (II) in the Karlin compound. $^{16}O-^{16}O$ intraperoxide stretch 800 cm^{-1}

(2)

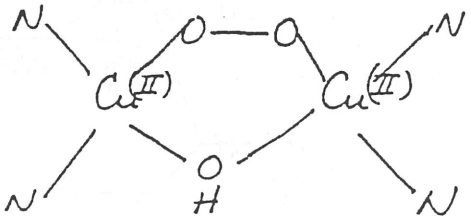

Bridging end-on cis-μ-1,2 peroxo model

a) overlap with second Cu(II) stabilizes the π^*_σ orbital of the peroxide, increasing the energy of the $\pi^*_\sigma \rightarrow$ Cu(II) $d_{x^2-y^2}$ charge transfer transition and increasing the intensity. This interaction also significantly raises the energy of $d_{x^2-y^2}+d_{x^2-y^2}$ orbital vis a vis $d_{x^2-y^2}-d_{x^2-y^2}$ orbital

b) HOMO ($d_{x^2-y^2}-d_{x^2-y^2}$) relatively non-bonding relative to peroxide